Dalton Transactions

Accepted Manuscript

ROYAL SOCIETY OF CHEMISTRY

www.rsc.org/dalton

Cu^{II} Bis(oxamato) End-grafted Poly(Amidoamine) Dendrimers†

Karoline Rühlig,[a] Robert Mothes,[a] Azar Aliabadi,[b] Vladislav Kataev,[b] Bernd Büchner,[b] Roy Buschbeck,[a] Tobias Rüffer,[a*] and Heinrich Lang[a]

[a] *Technische Universität Chemnitz, Faculty of Natural Sciences, Institute of Chemistry, Inorganic Chemistry, 09107 Chemnitz, Germany*

[b] *Leibniz Institute for Solid State and Materials Research IFW Dresden, Helmholtzstraße 20, 01069 Dresden.*

† Electronic supplementary information (ESI) available. Figures S1-S7 display IR Spectra, Figures S8–S10 show used NMR numbering scheme, Figures S11–S48 give ^{1}H, $^{13}C\{^{1}H\}$, $^{1}H,^{1}H$-COSYGPSW, $^{1}H,^{13}C$-HMBCGP and HSQCETGP NMR spectra, Figures 49 – 62 give ESI-MS spectra, Figure S63 shows UV/Vis spectra of **9c** and **10c** in H_2O and DMSO and Figure S64 gives variable temperature X-band EPR spectra of **10c**.
CCDC 1415744 (**Cu-3**) and 1415745 (**Ni-3**). For ESI and crystallographic data in CIF or other electronic format see DOI: xx.xxxx/xxxxxxx

Received,

Successive treatment of the diethyl ester of 3,4-bis(oxamate)phenylene benzoic acid (3,4-bopbH_2Et_2OH; **1**) with $[Bu_4N]OH$ and $MCl_2{\cdot}nH_2O$ (M = Cu, Ni; *n* = 2, 6) gave, upon extraction into CH_2Cl_2, the binuclear complexes $[Bu_4N]_4[\{M(3,4\text{-bopbO})\}_2CH_2]$ (**M-3**, M = Cu, Ni) as novel symmetric methylene diesters. In contrast, subsequent addition of $[Bu_4N]OH$ and anhydrous $NiCl_2$ to **1** afforded the very hygroscopic $[Bu_4N]_3[Ni(3,4\text{-bopbO})]$ (**4**) instead. In order to verify reaction conditions to achieve the to **1** corresponding carboxamides – as a crucial step for the synthesis of higher generations dendrimers - **1** was shown to react with RNH_2 (R = Me (**5a**), Pr (**5b**)) to $[RNH_3][tdqc]$ (R = Me (**6a**), Pr (**6b**); tdqc = 1,2,3,4-tetrahydro-2,3-dioxo-6-quinoxaline carboxylate) by rearrangement reactions. Alternatively, if **1** was converted first to 3,4-bopbH_2EtF (**8**) and treated next with $PrNH_2$, the corresponding carboxamid 3,4-bopbH_2Et_2NPrH (**7b**) could be obtained in high yields. The reaction of **7b** with $[Bu_4N]OH$ and $MCl_2{\cdot}nH_2O$ (M = Cu, Ni; *n* = 2, 6) gave conveniently mononuclear $[Bu_4N]_2[M(3,4\text{-bopbNPrH})]$ (**M-9b**, M = Cu, Ni). After thus optimizing reaction conditions,

for the synthesis of higher-branched bis(oxamato) type complexes, the (polyamido)amines **5c** ($en^{II}H_2$), **5d** ($den^{III}H_3$), **5e** ($den^{V}H_5$) and **5f** ($den^{X}H_{10}$), possessing two, three, five or ten terminal amino groups were reacted with appropriate equivs of **8** to give the corresponding carboxamides en^{II}(3,4-bopbH$_2$Et$_2$)$_2$ (**7c**), den^{III}(3,4-bopbH$_2$Et$_2$)$_3$ (**7d**), den^{V}(3,4-bopbH$_2$Et$_2$)$_5$ (**7e**) and den^{X}(3,4-bopbH$_2$Et$_2$)$_{10}$ (**7f**). Compounds **7c**–**f** were converted to the corresponding Cu^{II}-containing complexes **9c-f**, which were treated with corresponding equivs of [Cu(pmdta)][BF$_4$]$_2$ to afford **10c-f**. Complexes of the series **9c**–**f** and **10c-f** possess two, three, five or ten end-grafted mononuclear {Cu(3,4-bopb)}$^{2-}$ and trinuclear {Cu$_3$(3,4-bopb)(pmdta)$_2$}$^{2+}$ complex fragments, respectively.

The identities of **7c**–**f** were established by NMR spectroscopy and ESI-MS measurements. For **9c**–**f** and **10c**–**f**, ESI-MS, UV/Vis and ESR studies were applied to confirm the identities of these species. The magnetic properties of the {Cu$_3$(3,4-bopb)(pmdta)$_2$}$^{2+}$ end-grafted poly(amidoamine) dendrimers **10c**–**f** were studied by susceptibility measurements *vs* temperature to give *J* values between −112 (**10c**) to −118 cm^{-1} (**10d**), which are typically observed for discrete trinuclear Cu^{II}-containing bis(oxamato) type complexes.

Introduction

Dendrimers are regularly and repetitively branched macromolecules of well-defined size.[1–5] As a consequence of the dendritic architecture, thus, in dependency of the dendrimer generation, several unique physico-chemical properties or trends were observed, which have been described by the term “dendritic effect”.[6,7]

Within this terminology between a positive or negative dendritic effect can be distinguished if the impact to such a property is increased or decreased.[5,7] Dendritic effects have been, for example, shown and explained multiple times for catalytic reactions,[8–11] the inclusion of guest molecules[12,13] and for electrochemical properties.[7,14–18] Dendritic effects can originate from the presence of multiple functional groups in the interior of such a macromolecule by, for example, influencing the interactions with guest molecules.[7,12,19,20]

On the other hand, the physical size of the dendritic surface can also induce dendritic effects, since it may act as a shield to inhibit certain physico-chemical processes of the internal functionalities. Thus, it is possible to influence the shape of the dendrons by different solvents, so that the branches can be sprawled to form open structures, or the branches are more folded, adopting a more compact structure.[7]

Furthermore, cooperative effects due to the close proximity of terminal groups can generate dendritic effects in particular for catalytic reactions. Cooperativity between catalytically active functional groups can bring those sites in vicinity and thus a high local concentration of catalytically active species are available, which changes the activity in comparison to the isolated functionality.[11,21–23]

In case that magnetically active complex fragments are bound as terminal functionalities to dendrimers, such molecules may display dendritic effects as well. Additional and/or modified magnetic exchange interactions might be observed, or, the magnetic properties of such molecules could be just the sum of all individual end-grafted (para)magnetic entities. Such molecules could be then referred as "magneto dendrimers". However, up to now dendrimers were just "loaded" by magnetic metal and/or metal oxide nanoparticles as guests.[24–26] Additionally, dendrimers have been "decorated" with paramagnetic Cu^{II} or Gd^{III} ions, or combinations of both metal ions.[27–31] In this respect, polyamido amine (PAMAM) dendrimers have been widely used for stabilization of nanoparticles and metal ions and are often the dendrimer type of choice.[24,32,33] Such materials facilitates their use as data storage materials,[34–36] MRI contrast agents[30,31,37–40] and even as catalysts for environmentally sensitive reactions.[33,41,42]

PAMAM dendrimers with their terminal $–NH_2$ groups can be easily bound to carbon acid derivates. If such derivates possesses suitable donor functionalities, paramagnetic transition metal ions could be coordinated. For example, 3,4-bopbH_2Et$_2$OH (**1**), a bis(oxamate) type molecule,[43] could be bound to the periphery of PAMAM dendrimers of different generations to allow the formation of corresponding (multinuclear) bis(oxamato) type complexes. Indeed, bi-, tri- and even polynuclear bis(oxamato) type complexes have been already shown to be very useful materials for exploring magnetic exchange interactions.[44–48]

Moreover, special designed bis(oxamate) or oxamate type molecules did allow to coordinate at least two transition metal ions, and such precursors were used by the so-called "complex-as-ligand/complex-as-metal strategy" to fabricate higher nuclear complexes (Figure 1).[49] Selected representatives have been already referred as "high-spin dendrimer-like"[50] (**{CuM'$_2$}$_2$-a**, Figure 1) or even as "first-generation metallo-dendrimers" (**{M^{II}Cu$^{II}_2$}-{Cu^{II}Cu$^{II}_2$}$_2$-o**, Figure 1).[49–68]

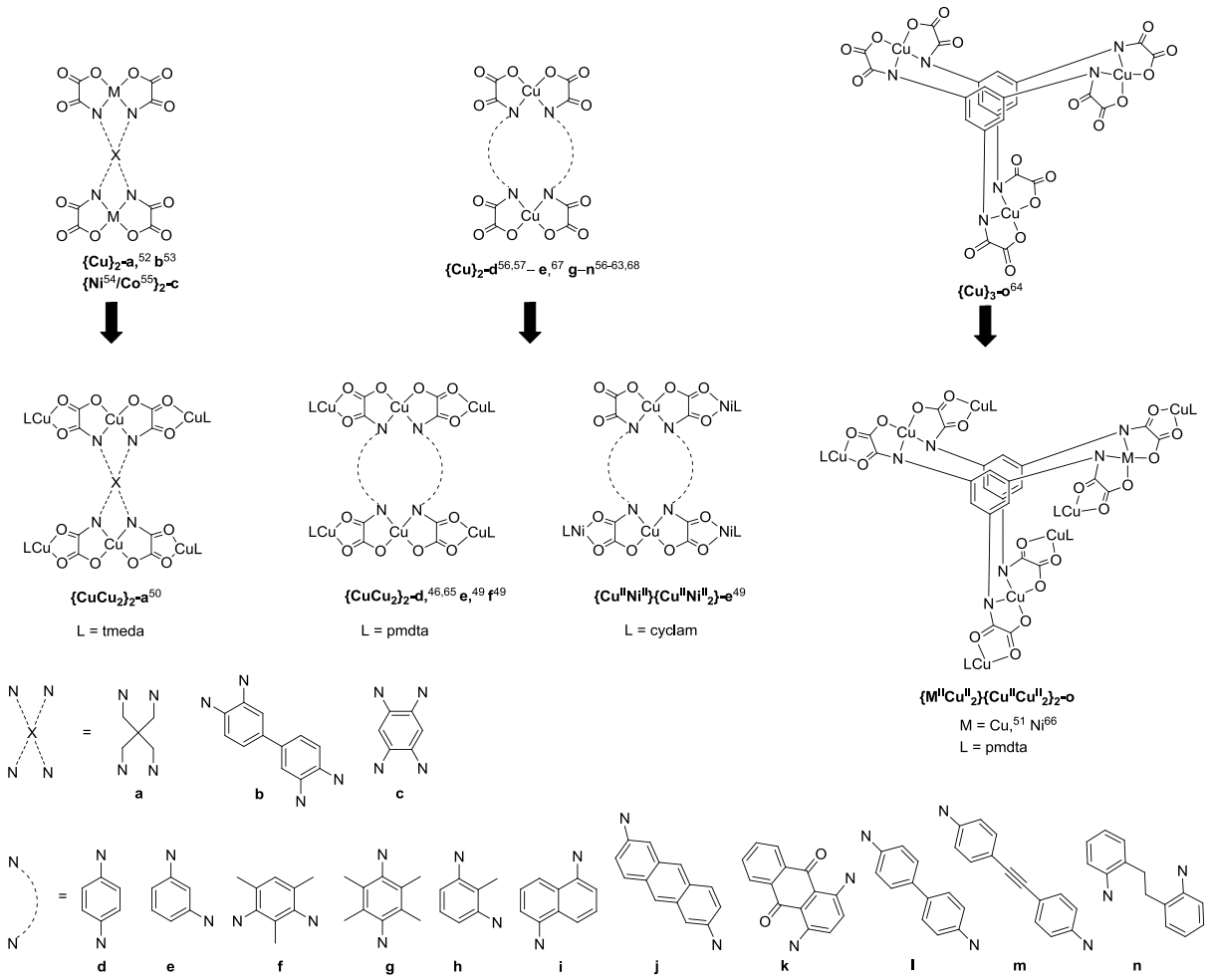

Figure 1. Chemical structures of crystallograhically characterised $\{M^{II}\}_n$- and $\{M^{II}M'^{II}_2\}_n$-type bis(oxamato) complexes (tmeda = *N,N,N',N'*-tetramethylethylene diamine, pmdta = *N,N,N',N'',N''*-pentamethyldiethylene diamine, cyclam = 1,4,8,11-tetra-azocyclotetradecane).

For complexes **{Cu}$_2$-a** or **{Cu}$_3$-o** (Figure 1) magnetic exchange interactions were observed.[50,64] Their corresponding $\{M^{II}M'^{II}_2\}_n$-type species, *e.g.* $\{Cu^{II}Cu^{II}_2\}_2$**-o** or $\{Ni^{II}Cu^{II}_2\}\{Cu^{II}Cu^{II}_2\}_2$**-o**, display then additional magnetic exchange interactions and even local anisotropies,[50] due to intramolecular magnetic exchange interactions.[66]

With the aim to bring trinuclear bis(oxamato) type complex fragments into spatial proximity and to investigate, whether this may induce additional magnetic exchange interactions or not, we set-out to terminate PAMAM dendrimers of different generations with 3,4-bopbH_2Et$_2$O groups. Their conversion to complexes with engrafted $\{M^{II}\}_n$ and $\{M^{II}M'^{II}_2\}_n$ bis(oxamato) entities is reported together with the magnetic characterization of the last-mentioned complexes.

Results

Synthesis

Optimising peptide coupling reaction conditions: One possibility to attach bis(oxamate) functionalities to $-NH_2$ endgrafted PAMAM dendrimers is given via the peptide coupling of them with the diethyl ester of *o*-phenylene-bis(oxamic acid) (3,4-bopbH_2Et_2OH, **1**). Alternatively, the Cu^{II} complex of **1**, for example in form of its tetrabutylammonium salt, $[Bu_4N]_2$[Cu(3,4-bopbOH], could be used for the peptide coupling reaction as well. In order to verify the accessibility of bis(oxamato) complexes of **1**, it was treated with 5 equiv. of $[Bu_4N]OH$, followed by the addition of the appropriate Cu^{II} and Ni^{II} salts (Scheme 1). Standard synthetic procedures were applied,[69] with the exception of the use of five instead of four equiv. of OH^-. By making use of $[Bu_4N]OH$, the corresponding complexes become well-soluble in CH_2Cl_2.[70] Thus, extraction of the reaction mixtures with CH_2Cl_2, followed by washing the organic phase with H_2O did give the respective pure bis(oxamato) complexes **Cu-3** and **Ni-3** (Scheme 1) in high yields.[70] This finding is surprising, as **Cu-3** and **Ni-3** represents easily achievable symmetric methylene diesters. The number of crystallographically characterized examples is small[71–73] and, moreover, their synthesis usually requires much harder reaction conditions.[73,74] For further discussions including the crystallographic characterization and discussions of the molecular structures cf. S65†.

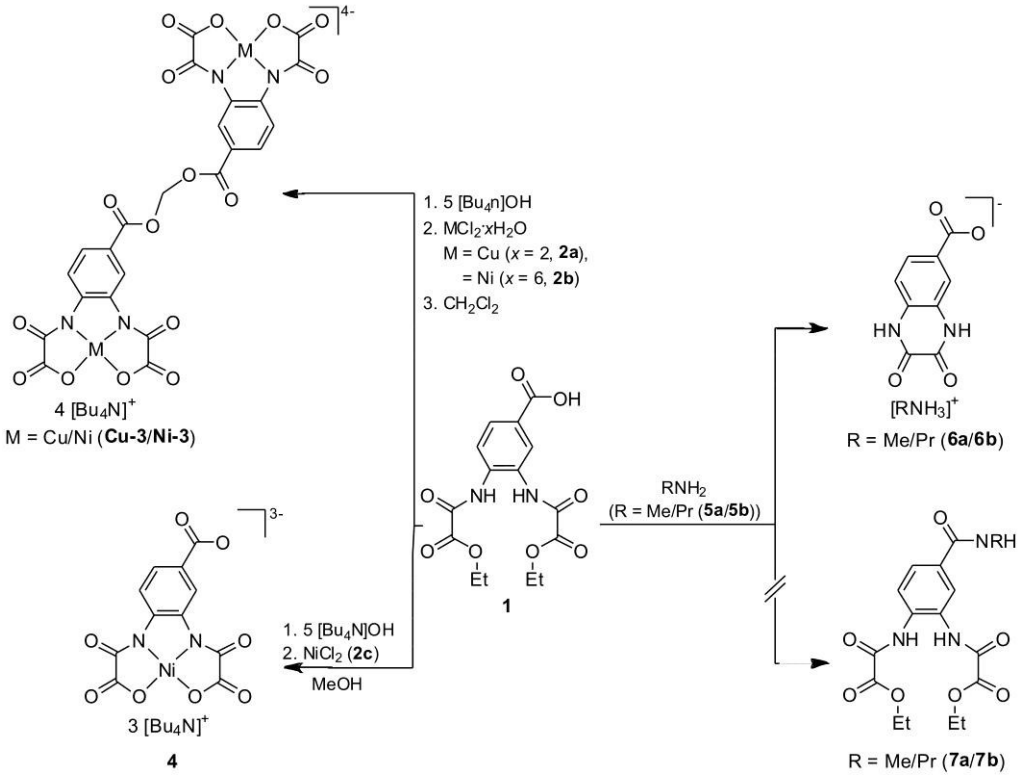

Scheme 1. Synthesis of **Cu-3**, **Ni-3**, **4** and **6a**,**b** from **1**.

In order to avoid a reaction with CH_2Cl_2, **1** was thus treated as shown in Scheme 1 to give **4** in a reasonable yield, but as a very hygroscopic material. It turned out that this complicates to use **4** or, alternatively, **4** in form of its protonated version as $[Bu_4N]_2$[Ni(3,4-bopbOH], for peptide coupling reactions. To investigate and mimic reaction conditions for the peptid coupling of **1** to $-NH_2$ endgrafted PAMAN dendrimers, it was tried to convert **1** into its corresponding carboxamides by simple addition of primary amines RNH_2 (Scheme 1). The addition of only one equiv. of RNH_2 to **1** forms salts of the composition $[RNH_3]$[3,4-bopbH_2Et_2O], which are not further reported here. By using an excess of $R–NH_2$, however, a rearrangement reaction occurs to give the quinoxaline-2,3-diones **6a** and **6b** (Scheme 1). Analogous rearrangements have been already observed, either by the exclusive treatment of diethyl bis(oxamates) with amines,[75] or in course of trials to convert them to bis(oxamato) type complexes.[76]

A more promising synthetic methodology to synthesize **7b** is given by a subsequent reaction route (Scheme 2): Addition of cyanuric fluoride to **1** in the presence of pyridine (reaction path (*i*)),[77,78] or treatment of **1** with 70-% HF·py and DCC (= *N*,*N'*-dicyclohexylcarbodiimide) (reaction path (*ii*)),[79,80] gave 3,4-bopbH_2Et_2OF (**8**) in good yields. Reaction of **8** with $PrNH_2$ (**5b**) in the presence of pyridine afforded then **7b** successfully in high yields. To verify the reaction conditions for the synthesis of mononuclear bis(oxamato) type complexes, **7b** was treated by standard procedures as described above to give **Cu-9a** and **Ni-9b**, respectively.[69,70] The identities of both complexes were established unambiguously, although unfortunately single crystals of them were not of required quality for single crystal X-ray diffraction studies. Nevertheless, the formation of **Cu-9b** and **Ni-9b** by standard procedures indicates that especially the carboxamide functionality of **7b** does not undergo any derivatisation in course of this reaction.

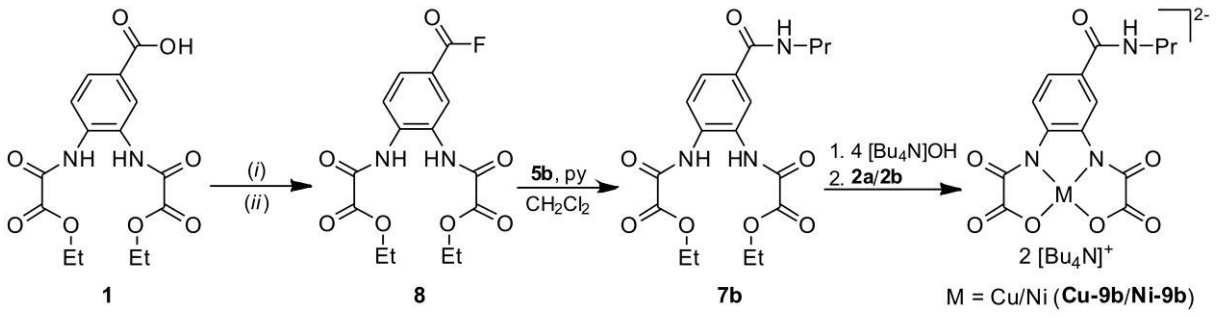

Scheme 2. Synthesis of **Cu**/**Ni-9b** via **8** and **7b**. (*(i)* $C_3N_3F_3$, CH_2Cl_2, py, 0 °C; *(ii)* $(HF)_x$·py (70%), DCC, CH_2Cl_2, 25 °C). (DCC = *N*,*N'*-dicyclohexylcarbodiimide)

*Perfoming peptide couplings of **8** with –NH_2 endgrafted PAMAM dendrimers and subsequent metallation reactions*: After verifying the peptide coupling conditions (Scheme 2) ethylenediamine ($en^{II}H_2$, **5c**) and the PAMAM dendrimers $den^{III}H_3$ (**5d**), $den^{V}H_5$ (**5e**) and $den^{X}H_{10}$ (**5f**) (Figure 2), should be reacted with **8** under analogous reaction conditions as described above. Before, **5d** and **5e** were prepared according a divergent synthetic procedure first described by Tomalia *et al.*[81,82] Compound **5f**, that possesses ten endgrafted –NH_2 groups per molecule (Figure 2), was obtained from **5e** by addition of methylacrylate and **5c** in MeOH. The unambiguous identities of **5d**–**f** were checked by NMR spectroscopy, elemental analysis and IR spectroscopy (Experimental Section).

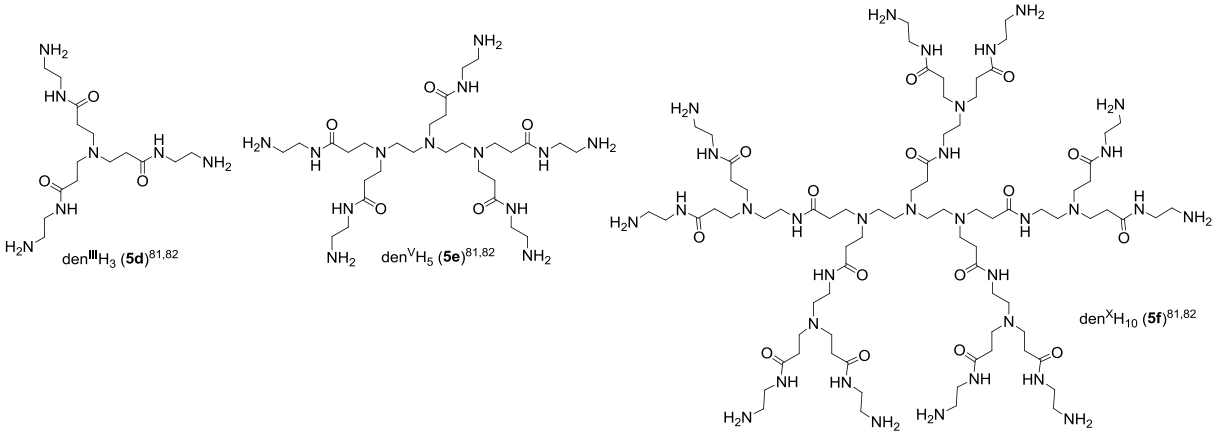

Figure 2. Chemical structures of the polyamidoamine (PAMAM) dendrimers **5d**–**f**.

For the synthesis of **7c** (Figure 3), $en^{II}H_2$ (**5c**) was reacted with the precise stoichiometric amount of **8**. Compound **7c** could be isolated by an aqueous work-up and was obtained analytically pure in good yields. In case of the synthesis of **7d**,**e** (Figure 3) out of $den^{III}H_3$ (**5d**) and $den^{V}H_5$ (**5e**) it turned out that an excess of **8** (**7d**, 10 %; **7e**, 5 %) is required in order to perform all individual peptide coupling steps perfectly. The larger the excess of **8**, the sooner **7d**,**e** are formed, but the more complicated is the isolation of analytically pure materials. Starting with **7d**, an aqueous work-up is not reasonable anymore, as the dendrimers could not be obtained free of water and of $NaHCO_3$ (with varying contents). Both pollutants might interact with the dendrimers by, *e. g.*, formation of hydrogen bonds or might be filled into dendrimer cavities, especially the larger the dendrimer is.[83,84] Instead, **7d**,**e** were filtered off after the peptide coupling reaction, washed excessively with Et_2O and thf and dried for prolongated times in vacuum. That work-up guarantees to remove the excess of **8**. However, for **7e** it was noted that remaining amounts of CH_2Cl_2, the solvent used for the peptide coupling, could not be removed. This is somewhat surprising and might be attributed to its capturing in dendrimer cavities of **7e**.[83,84] In case of the synthesis of **7f** out of $den^{X}H_{10}$ (**5f**) and **8** more severe problems were noted. The finally chosen excess of **8** (3.5 %) is here the

best compromise between achieving **7f** with all individual peptide coupling steps being performed and a reasonable purity. Lowering the excess of **8** further does not guarantee all peptide couplings to be happen. However, the work-up procedure used as described for **7d**,**e** did not give **7f** analytically pure, as the excess of **8** could not be liberated (Experimental Section). This is attributed to interactions of **8** with **7f** as outlined above and prompted us to abstain from the synthesis of higher generation dendrimers. Nevertheless, the excess of **8** in **7f** does not seem to hamper the synthesis and purity of Cu^{II} complexes of **7f**, as described below.

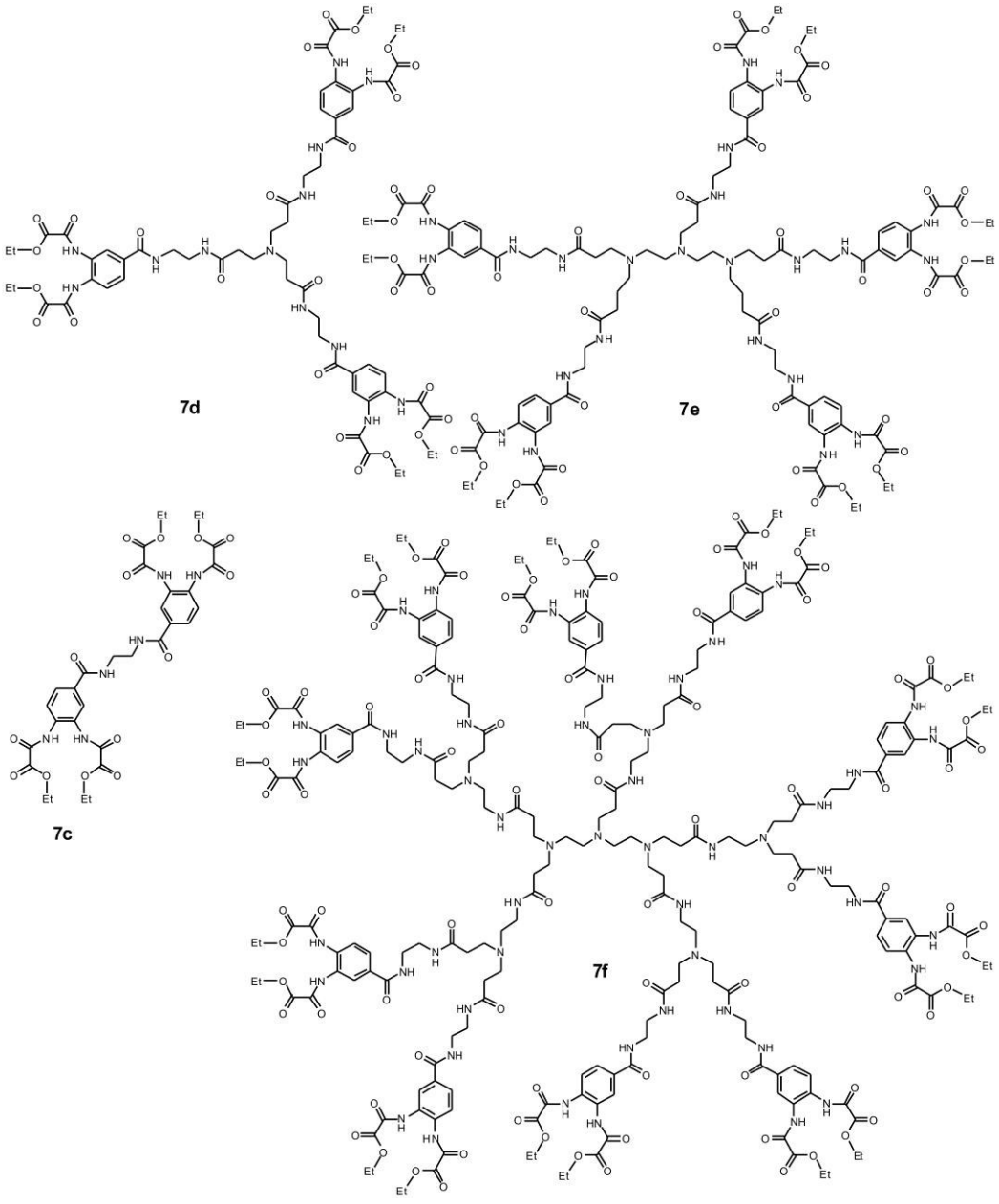

Figure 3. Chemical structures of **7c**–**f**.

The Cu^{II} complexes **9c**–**f** (Figure 4) were obtained by treatment of **7c**–**f** with appropriate equiv. of $[Bu_4N]OH$ and **2a**, as described above for **Cu-9b**. As they were all extracted into CH_2Cl_2, it is assumed that the remaining of amount of **8** in **7f** is converted to **Cu-3**, which is

very well soluble in both CH_2Cl_2 and MeCN. Out of the CH_2Cl_2 solutions, **9c**–**f** were precipitated by addition of thf/Et_2O. Especially for **9f** the addition of thf/Et_2O was stopped at a point, where the remaining solution was still purple coloured. In the same way **9f** was precipitated from MeCN. In doing so, it is assumed that disturbing **Cu-3** is stripped away at the expense of the yield of **9f**, which is comparatively low. Indeed, the IR spectra of **9f** (Figure S6†) does not indicate any presence of **Cu-3** (Figure S1†).

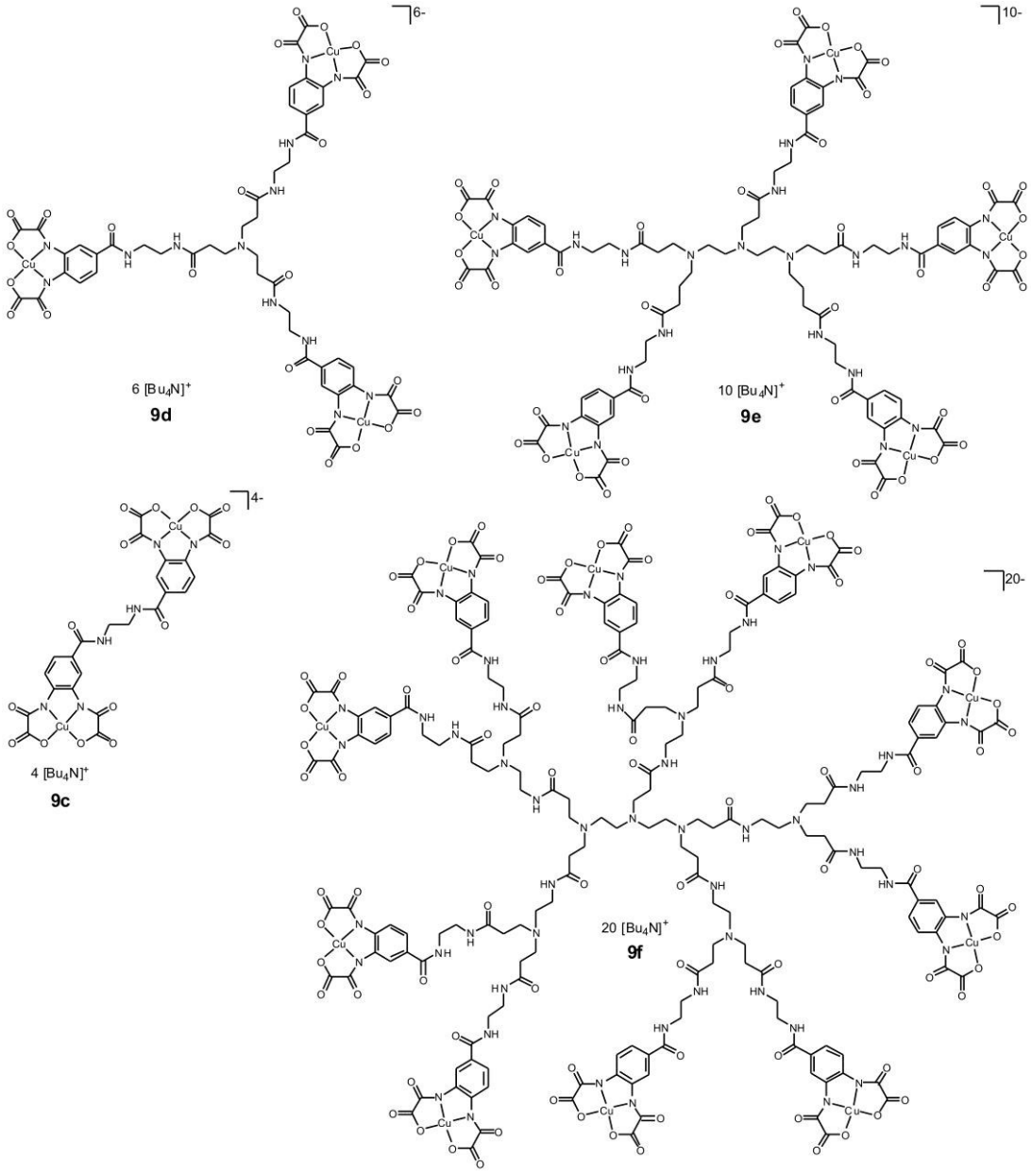

Figure 4. Chemical structures of **9c–f**.

By reacting **9c**–**f** with appropriate equiv. of [Cu(pmdta)][$(BF_4)_2$] (**2d**) in MeCN the compounds **10c**–**f** (Figure 5), carrying *n* endgrafted trinuclear $\{Cu_3(3,4\text{-bopb})(pmdta)\}^{2+}$ entities (**10c**, *n* = 2; **10d**, *n* = 3; **10e**, *n* = 5; **10f**, *n* = 10) could be obtained in moderate yields. After reducing the reaction solution volume to 5 mL, **10c**–**f** were precipitated as green colored

solids by addition of thf. Thus obtained materials were purified further by multiple precipitations from a mixture of MeCN/DMF (ratio 5:2, *v/v*) and Et_2O (Experimental Section). It was observed that with each additional precipitation the compound became less soluble and hence the amount of DMF had to be increased. This relative simple purification methodology allowed the isolation of **10c**–**f** in pure form, however, at the expense of the yield (35 – 56 %) (Experimental Section).

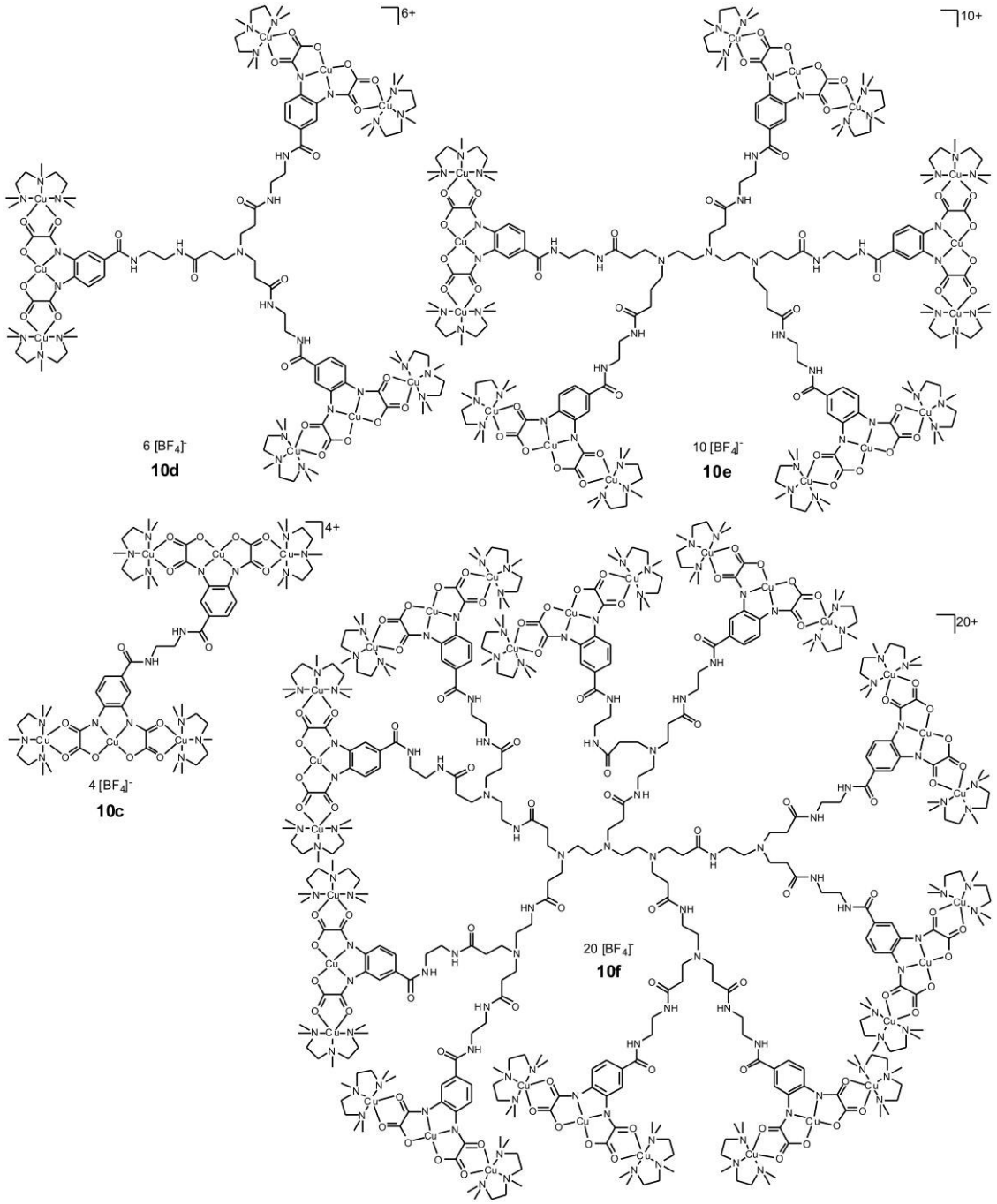

Figure 5. Chemical structures of the "magneto-dendrimers" **10c**–**f**, possessing two (**10c**), three (**10d**), five (**10e**) or ten (**10f**) endgrafted $\{Cu_3(3,4\text{-bopb})(pmdta)_2\}^{2+}$ complex fragments.

Characterisation

Structural descriptions: The molecular structures of **Cu-3** and **Ni-3** in the solid state have been determined by single-crystal X-ray diffraction analysis, whereby crystals were of the composition $[Bu_4N]_4[\{M(3,4\text{-bopbO})\}_2CH_2]\cdot{}^3/_2MeCN$ (M = Cu (**Cu-3**), Ni (**Ni-3**)). The molecular structures of the tetraanionic complex fragments are shown in Figure 6, together with selected bond lengths and angles in the Figure caption. As corresponding bond lengths and angles of each of the two individual complex fragments around the atoms Cu1 (**Cu-3**) and Ni1 (**Ni-3**), respectively, are not significantly different, only the ones around Cu1 and Ni1 are given and discussed further. Crystal/structural refinement data are summarized in Table S 1†.

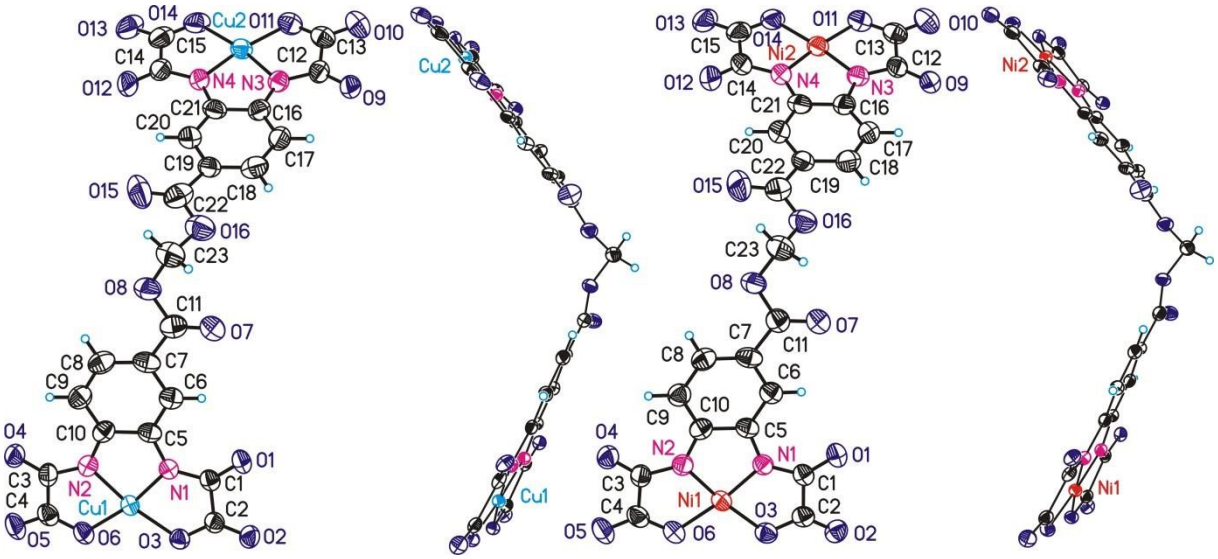

Figure 6. ORTEP diagram (50% probability level) of the molecular structure of **Cu-3** (left) and **Ni-3** (right) in two different perspective views. All $[Bu_4N]^+$ cations and MeCN packing solvent molecules are omitted for clarity. Selected bond lengths (Å) and angles (°) of **Cu-3** (M = Cu)/**Ni-3** (M = Ni): M1–N1 1.896(2)/1.817(3), M1–N2 1.911(2)/1.830(3), M1–O3 1.951(2)/1.894(2), M1–O6 1.937(2)/1.882(2), N1–C1 1.333(4)/1.335(4), N1–C5 1.398(4)/1.406(4), N2–C3 1.336(4)/1.339(4), N2–C10 1.392(4)/1.395(4), C1–C2 1.570(5)/1.558(5), C3–C4 1.553(5)/1.550(5), O1–C1 1.228(4)/1.230(4), O2–C2 1.223(4)/1.222(4), O4–C3 1.231(4)/1.238(4), O5–C4 1.229(4)/1.228(4), O3–C2 1.299(4)/1.298(4), O6–C4 1.296(4)/1.287(4), C11–O7 1.193(4)/1.209(4), C11–O8 1.386(4)/1.379(4), C23–O8 1.437(5)/1.429(4); N1–M1–N2 84.14(11)/86.37(12), N1–M1–O3 84.93(10)/86.24(11), O3–M1–O6 106.06(10)/101.19(10), N1–M1–O6 168.92(11)/172.50(11), N2-M1-O3 168.99(10)/172.47(11), N2-M1-O6 84.90(11)/86.23(11).

A common feature of **Cu-3** and **Ni-3** is the coordination of the 3,4-bopbO^{4-} ligands to the respective metal ion by the two amido nitrogen atoms N1 and N2 and by the two carboxylato oxygen atoms O3 and O6, forming planar-trapezoidal MN_2O_2 coordination units. The planarity of the MN_2O_2 units is nicely expressed by minor deviations of calculated mean planes of the atoms N1, N2, O3 and O6 with root mean square deviations (rmsd) from planarity for **Cu-3**/**Ni-3** of 0.022/0.020 Å. Additionally, the respective metal ions are placed 0.003(1)/0.002(1) Å above the calculated mean planes of **Cu-3**/**Ni-3**. This $\eta^4(\kappa^2N,\kappa^2O)$

coordination of bis(oxamato)[47] or the $\eta^4(\kappa^4N)$ coordination of related bis(oxamidato) type ligands[94] to a central metal ion is usually observed, although exceptions have been described.[95,96] Furthermore, the {M(3,4-bopbO)} complex fragments of **Cu-3** and **Ni-3** can be considered as nearly planar. Calculated mean planes of the atoms M1, C1–C10, O1–O6, N1, N2 gave small deviations from planarity only for **Cu-3** (M1 = Cu1, rmsd = 0.054 Å) and **Ni-3** (M1 = Ni1, rmsd = 0.056 Å).

In agreement with observations made for related Cu^{II}- or Ni^{II}-containing bis(oxamato) type complexes,[97] for **Cu-3** the Cu1–N1/Cu1–N2 distances (1.896(2)/1.911(2) Å) are significantly shorter when compared to the Cu1–O3/Cu1–O6 distances (1.951(2)/1.937(2) Å) (Figure 6). A related tendency is observed for **Ni-3** with *d*(Ni1–N1/Ni1–N2) = 1.817(3)/1.830(3) Å *vs* *d*(Ni1–O3/Ni1–O6) = 1.894(2)/1.882(2) Å. According to Cervera *et al.*,[88] these observations are due to the greater basicity of the N (amide) compared to the O (carboxylate) donor atoms. On the other hand, this observation is due to the shorter ionic radius of Ni^{II} compared to Cu^{II} ions in planar coordination environments (Ni^{II}: 63 pm *vs* Cu^{II}: 71 pm).[98]

NMR spectroscopic measurements: In selected cases, for the appropriate assignment of chemical shifts of compounds under investigation, additional 2D NMR experiments (*$^1H,^1H$-Cosy*, *$^1H,^{13}C$*-HSQCETGP and HMBCGP) were carried out (Experimental Section, Figures S11–48†). Selected features of the NMR spectra did then help to assign the compounds and/or the progress of the reactions free of doubt: Distinctive in the ^{1}H NMR spectrum of **3b** is the appearance of the methylene bridge at 6.04 ppm and characteristic for **7** and **8** are the signals of the OEt, NH, RNH and C_6H_3 groups with their typical coupling pattern (Experimental Section). In addition, ^{1}H NMR spectroscopy allows monitoring the carboxamide formation. The intensities of the ^{1}H NMR signals of the terminal $-NH_2$ groups of **5c–f** gradually decline in course of the reaction to **7c–f** and consequently their full disappearance reveal complete conversions. Furthermore, the number of end-grafted diethyl ester bis(oxamic acid) entities in **7c**–**f** can be determined by comparing the integral ratio of the resonance signals of the C*H*$_3$ group with the inner NC*H*$_2$C*H*$_2$NH or NC*H*$_2$C*H*$_2$C(O) dendritic core units, allowing to confirm that in **7c–f** no surface defects are present. Potentially, within **7c–f** multiple intra- and/or intermolecular hydrogen bonds could be generated and these compounds might form different *cis*-*trans* isomers. As a consequence, the free rotation within the molecules is limited and broadened ^{1}H NMR signals are detected with increasing molecule size. An almost precise assignment of individual organic groups to their NMR resonance signals could thus not be carried out in all cases (Experimental Section).

Electrospray ionisation mass spectra: Measurements were performed for **7c–f**, **9c–f** and **10c–f** (Figures S49–62†). For all compounds, except **9f**, the ESI-MS data measured in positive or negative ionisation mode could be evaluated and ion peaks were assigned to isotope distribution patterns, confirmed by the proposed elemental composition and charge state (Experimental Section). Dendrimer **9f** was measured with positive and negative ionisation mode but the obtained ion peaks could not be assigned to any molecular fragments (Figure S58†). Slight deviations between measured and calculated distribution patterns of some samples , *e.g.* **10e** (Figure S61†) are reasoned in the low intensity of the obtained peaks.

Compounds **7c–f** show next to fragmentation peaks molecular ion peaks of general formula $[\mathbf{M} + n\mathrm{H}]^{x+}$ at *m/z* = 729.2362 (**7c**, *x* = 1) , 1362.5121 (**7d**, *x* = 1), 1173.4715 (**7e**, *x* = 2), 1032.4263 (**7f**, *x* = 5), proving the existence of the targeting dendritic molecules with two to ten endgrafted diethyl ester bis(oxamic acid) units. With exception of **9e** (*m/z* = 2635.7549, $[\mathbf{9e} + 2\mathrm{H}]^{2+}$) for **9c–e** and **10c–f** the respective molecular ion peaks were not observed. Nevertheless, it is possible to allocate additional ion peaks to molecule fragments of them (Experimental Section). Thereby, it was possible to assign for **9c–e** and **10c** ion peaks to fragments carrying the predicted number of Cu^{II} ions at *m/z* = 1462.7529 ($[\mathbf{9c} - Bu_4N]^-$), 1170.5743 ($[\mathbf{9d} - 2Bu_4N]^{2-}$), 2515.1162 ($[\mathbf{9e} + Bu_4N + H]^{2+}$) and 420.5928 ($[\mathbf{10c} - 4BF_4]^{4-}$), respectively (Experimental Section).

UV/Vis measurements: Electronic absorption spectra of **Ni-3**, **Cu-3**, **Cu-9b**, **Ni-9**, **9c–f** and **10c–f** were measured in solvents as indicated below. The ones of **Ni-3**, **Cu-3**, **Cu-9b** and **Ni-9b**, measured between 200–900 nm in MeCN (Figure 7), are discussed first.

For aromatic hydrocarbons a series of different absorptions are expected to appear (*α*, *p*, *β*, *β'* and *τ* UV band),[85,86] and for carbonyl groups as well (saturated: 280 nm, $\approx 10 < \varepsilon < \approx 110$, $n \rightarrow \pi^*$; *α*,*β*-unsaturated: 220–260 nm, $\varepsilon \approx 10000$, $\pi \rightarrow \pi^*$; 320 nm, $\varepsilon \approx 100$, $n \rightarrow \pi^*$).[85] Depending on the aromatic substitution pattern individual absorptions can change their order, namely the *α* and *p* band. Additionally, both aromatic hydrocarbon and carbonyl absorptions can superimpose,[87] which might modify intensities and band positions. Concerning this, a precise assignment of the intense UV bands observed for **Cu**/**Ni-3** and **Cu**/**Ni-9b** to specific absorptions should not be done. Otherwise and as expected, comparing the UV/Vis spectra of **Cu**/**Ni-3** and **Ni-9b** with those of related $[Cu(opba)]^{2-}$ [88] and $[Ni(opba)]^{2-}$ [89] (opba = *o*-phenylenebis(oxamato)) complexes reveals that very analogues features were observed. For example, for square-planar Cu^{II}/Ni^{II} complexes absorptions due to d–d transitions are expected. Consequently, for $[Cu(opba)]^{2-}$ a weak absorption at 560 nm (270) is observed,

representing the envelope of different possible d-d transitions.[88] For **Cu-3** and **Cu-9b** weak absorptions at 564 (400) and 561 nm (210) were detected, respectively (Figure 7), which fits perfectly with data reported for $[Cu(opba)]^{2-}$.[88] For the corresponding Ni^{II} complexes **Ni-3**/**Ni-9b** d–d transitions in the range between 400–666 nm ($50 < \varepsilon < 500$), followed often by a more intense band between 333–434 nm, would be expected.[90] Indeed, for **Ni-9b** at ca. 476 nm (ca. 245) a shoulder on the low-energy tail of the intense UV band with λ_{max} at 363 nm was noticed. This agrees nicely with observations made for related $[Ni(opba)]^{2-}$ (465 nm (ca. 500))[89], although for **Ni-3** such an additional absorption (shoulder) could not be observed (Figure 7). The absorption band potentially to be observed between 333–434 nm[90] could not be observed, as in that range absorptions of the organic ligand occurs as well.

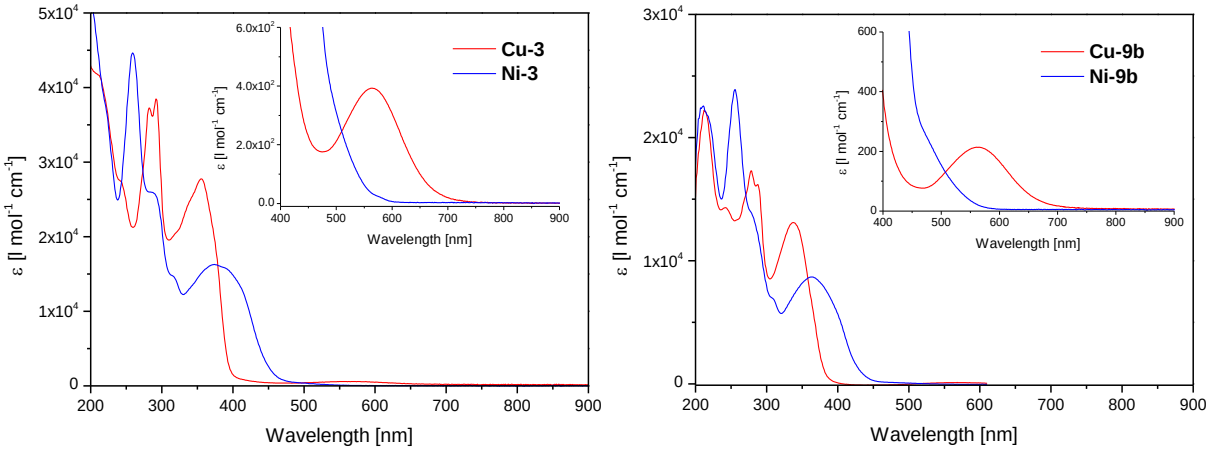

Figure 7. UV/Vis absorption spectra of Cu^{II}- and Ni^{II}-containing complexes **Cu-3** and **Ni-3** (left) and **Cu-9b** and **Ni-9b** (right) measured in MeCN.

For complexes **9c–f**, possessing two to ten individual endgrafted $\{Cu(3,4\text{-bopb})\}^{2-}$ units a related situation should be observed as discussed for **Cu-3** and **Cu-9b**, which is the case (Figure 8). Weak absorptions at around 560 nm were observed, representing the envelope of possible d–d transitions. Specific data are summarized in Table 1 (Discussion Section).

For complexes **10c–f**, possessing two to ten endgrafted trinuclear $\{Cu_3(3,4\text{-bopb})(pmdta)_2\}^{2+}$ entities, d–d transitions within the visible region are observed (Figure 8) as expected.[90–93] UV/Vis data for related discrete trinuclear Cu^{II} bis(oxamato) type complexes are sparingly reported, and indicate the appearance of only one broad absorption within the visible region around 620 nm in MeCN[91] or 650 nm in DMSO/H_2O[92] or DMF.[93] A related observation was made for **10c–f**, with one broad absorption band each at ca. 660 nm in DMSO (Table 1). The impact of the solvent was proven on the basis of **Cu-10c**, which is good soluble in MeCN and DMSO (Figure S63†). When changing the solvent from MeCN to DMSO a bathochromic shift of the d–d transition within the visible region was found from 638 nm (1215) to 658 nm (1308) which agrees with comments given above.

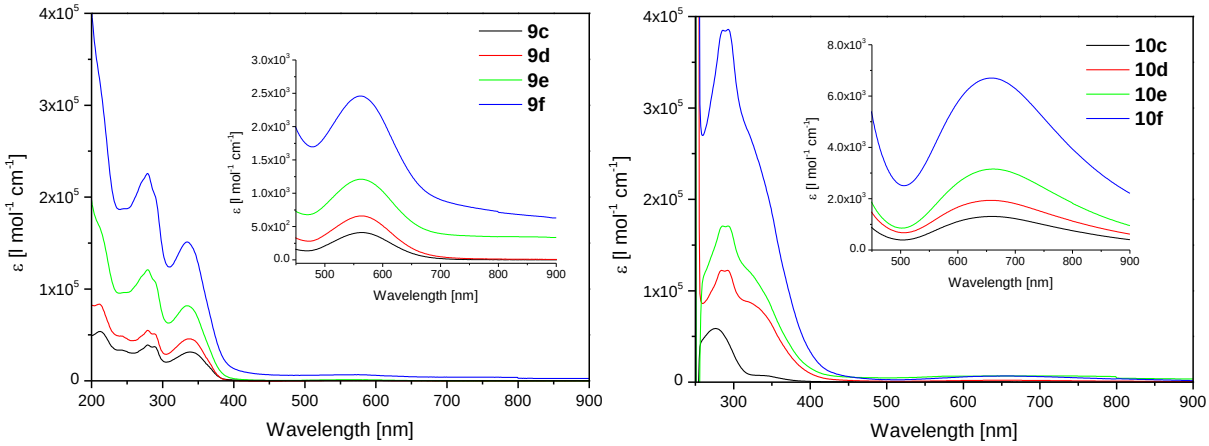

Figure 8. UV/Vis absorption spectra of **9c–f** (left, in MeCN) and **10c–f** (right, in DMSO).

ESR studies: ESR measurements have been carried out on powders of **10c–f** at a frequency f = 9.56 GHz (X-band) at different temperatures (Figure S64†). At each temperature, the ESR spectra of **10c–f** appear rather similar. At 4 K, the ESR spectrum shows a structured signal which peaks can be assigned to the three rhombic g-factors, g_1, g_2, and g_3, of the compound in the spin –½ doublet ground state (Table 1), as expected for a low symmetry ligand coordination of Cu^{II} in these samples. Remarkably, with increasing temperature line 1 is shifted to higher magnetic field, line 2 shows no significant shift and line 3 is shifted to lower magnetic field (Figure S64†). This effect can be attributed to a thermal population of the first excited doublet state possessing different g-tensor components. At high temperatures, the thermal relaxation effects broaden the lines and the g-tensor pattern is not resolved anymore. Such a temperature dependent change of the spectral shape is also observed for related discrete trinuclear Cu^{II} (bis)oxamato complexes, and is explained in terms of a progressive population of the excited spin states in the antiferromagnetically coupled spin trimer systems.[99,100] The temperature dependence of the integrated ESR intensity I_{ESR} in a temperature range T = 4–290 K and the corresponding inverse ESR intensities $1/I_{ESR}$ in a temperature range T = 4–60 K are presented in Figure 9. The values of I_{ESR} are normalized to the ideal proposed molecular weight and to the number n of endgrafted $\{Cu_3(3,4\text{-bopb})(pmdta)_2\}^{2+}$ entities per molecule of **10c–f**. With this normalization, the $I_{ESR}(T)$ and $1/I_{ESR}(T)$ curves practically overlap within the uncertainty of the measurement. For **10c**–**f**, the normalized inverse ESR intensity *vs* temperature $1/I_{ESR}$ shows a linear behaviour at T < 60 K similar to the dependence of the inverse static susceptibility $\chi_m^{-1}(T)$ in the same temperature range where it follows the Curie-Weiss law $\chi_m^{-1}(T) = (T+\theta)/C$ (Figure 9). Such a correspondence is expected since the ESR intensity is proportional to the static magnetic susceptibility of the spins participating in the resonance.

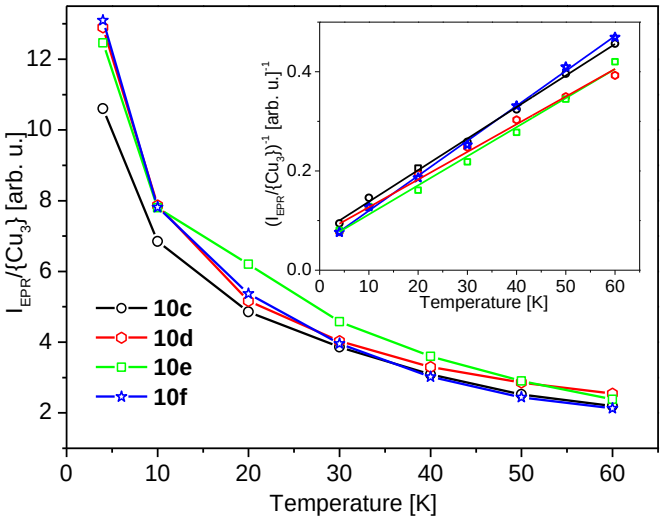

Figure 9. Temperature dependence of the integrated EPR intensity $I_{ESR}(T)$ (main panel) and its inverse $1/I_{ESR}(T)$ (inset) for **10c–f**. {Cu_3} abbreviates $\{Cu_3(3,4\text{-bopb})(pmdta)_2\}^{2+}$.

Magnetic properties: The temperature dependence of the static magnetic susceptibility χ_m = M/H and of the inverse susceptibility χ_m^{-1} for **10c–f** are presented in Figure 10. All compounds show the same temperature dependent behaviour. The $\chi_m^{-1}(T)$ dependence shows a strong bending at temperatures around 60–75 K, which is typical for discrete trinuclear Cu^{II}-containing (bis)oxamato type complexes possessing an antiferromagnetic interaction between the Cu^{II} spins S = ½.[97,100,101] The experimental data were fitted on the basis of the following Hamiltonian using the simulation software package julX[102]:

$$\hat{H}_{ex} = \sum_{i=1}^{3} g_i \mu_B H \cdot S_i - J_{12} S_1 S_2 - J_{23} S_2 S_3 \qquad (1)$$

Here, J_{12} and J_{23} denote the exchange coupling parameters between the central and the terminal Cu^{II} spins and the first term accounts for the Zeeman interaction. The magnetic exchange between the terminal Cu^{II} spins was assumed to be very small and thus neglected. Since the ESR data enable a conclusion on the absence of the magnetic interaction between the arms in the molecule, we have simulated the magnetic susceptibility *vs* temperature for individual $\{Cu_3(3,4\text{-bopb})(pmdta)_2\}^{2+}$ entities. For this purpose, the $\chi_m(T)$ curves of compounds **10c–f** were divided by the number n of these entities. A good agreement between experimental data and the fit of $\chi_m^{-1}(T)$ plot was observed in all cases, which further confirms absence of magnetic interaction between the $\{Cu_3(3,4\text{-bopb})(pmdta)_2\}^{2+}$ entities within the dendrimers. An exemplary fit for **10c** is shown in Figure 10. The J values resulting from the fit were determined to be –112 cm^{-1} (**10c**), be –118 cm^{-1} (**10d**), be –112 cm^{-1} (**10e**) and be –112 cm^{-1} (**10f**), respectively, cf. Table 1.

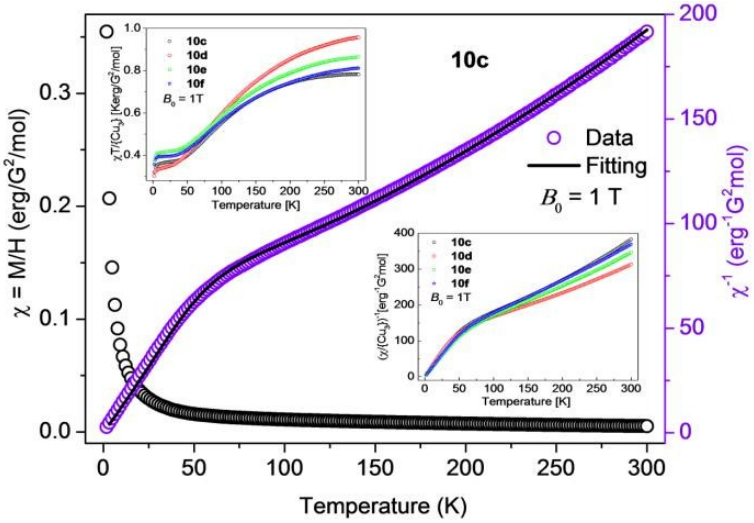

Figure 10. Main panel: Temperature dependence of the magnetic susceptibility χ = M/H and of the inverse suszeptibility χ^{-1} for **10c** (symbols) together with the fit according to Hamiltonian Eq. (1) (solid line). Insets: Temperature dependences of χT (left) and χ^{-1}(T) (right) for **10c–f** normalized to the number of $\{Cu_3(3,4\text{-bopb})(pmdta)_2\}^{2+}$ entities abbreviated as $\{Cu_3\}$.

Discussion

As already mentioned, dendrimers might display "dendritic effects" as a consequence of their architecture. The specific aim of this study was to bring trinuclear bis(oxamato) type complex fragments into spatial proximity and to investigate, whether this may induce additional magnetic exchange interactions in dependency of the dendrimer generation. As all before reported complexes have been characterized by UV/Vis, ESR and magnetic measurements, obtained results will be briefly summarized in order to discuss whether dendritic effects could be observed or not. Selected results of these measurements are summarized in Table 1.

UV/Vis studies: It is intriguing to notice that related absorptions of **Cu-3** and **Cu-9b** are approximately doubled in intensity, cf. Table 1 below. This should be the case, as **Cu-3** possesses two chromophores, compared to only one in **Cu-9b**. However, for **Cu-3** one would not expect to observe any dendritic effect when comparing with **Cu-9b**. On the other hand, a related comparison can be made for complexes of the two series **9c**–**9f** and **10c–f**, respectively, as well. Thus, in dependency of the number *n* of endgrafted mononuclear $\{Cu(3,4\text{-bopb})\}^{2-}$ (**9c**–**f**) or trinuclear $\{Cu_3(3,4\text{-bopb})(pmdta)_2\}^{2+}$ (**10c**–**f**) entities, the detected molar attenuation coefficients ε show a related increase in intensity (Table 1). This increase of ε is, however, nearly linear as the quotient of ε/n remains nearly the same, cf. Table 1. In consequence, no dendritic effects for the two series of Cu^{II}-containing bis(oxamato) end-grafted poly(amidoamine) dendrimers with respect to their UV/Vis absorption behaviour are observed, although the nearly identical ε/n quotients are an additional evidence of the identities of synthesized complexes.

Table 1. Summary of characterisation results of investigated complexes.

Complex	UV/Vis			ESR[d]				*J* values[d]
	λ_{max}	ε	ε/n[a]	g_1	g_2	g_3	g_{ave}	$J_{12} = J_{23}$ (cm^{-1})
Cu-3	564	393	197	–	–	–	–	–
Ni-3	-[b]	-[b]	-[b]	–	–	–	–	–
Cu-9b	565	214	214	–	–	–	–	–
Ni-9b	ca. 476	245	245[c]	–	–	–	–	–
9c	563	411	206	–	–	–	–	–
9d	562	660	220	–	–	–	–	–
9e	563	1212	242	–	–	–	–	–
9f	562	2460	246	–	–	–	–	–
10c	658	1308	654	2.226	2.101	1.995	2.112	–112
10d	658	1935	645	2.231	2.102	1.985	2.091	–118
10e	661	3155	631	2.228	2.102	1.988	2.091	–112
10f	658	6703	670	2.225	2.102	1.991	2.091	–112

[a] *n* refers to the number of $\{Cu(3,4\text{-bopb})\}^{2-}$ and $\{Cu_3(3,4\text{-bopb})\}^{2+}$ entities for **9c–f** and **10c–f**, respectively: *n* = 1 (**Cu-9b**), *n* = 2 (**Cu-3**/**9c**/**10**c), *n* = 3 (**9d**/**10d**), *n* = 5 (**9e**/**10f**), *n* = 10 (**9f**/**10f**). [b] No individual absorption was detected.[c] *n* refers to the number of $\{Ni(3,4\text{-bopb})\}^{2-}$ entities in **Ni-9b** (*n* = 1). D) . Principal values of the exchange coupling parameter *J* obtained from the Hamiltonian fit of $\chi_m^{-1}(T)$ and the three rhombic *g*-factors (g_1, g_2, and g_3) of **10c–f** in the spin –1/2 doublet ground state obtained by ESR spectra (4 K).

ESR studies: The slope of the $1/I_{ESR}(T)$ dependence, cf. Figure 9, is proportional to the inverse Curie constant *C* and thus to the inverse concentration of the resonating spins. The fact that this slope is very similar for **10c**–**f** suggests that all $\{Cu_3(3,4\text{-bopb})(pmdta)_2\}^{2+}$ units in the respective molecules contribute to the ESR signal within about 10% of uncertainly. The value of the Curie-Weiss temperature θ, as estimated from the $I_{ESR}(T)$ dependence, scatters between –7 and –12 K which can be ascribed to the limited accuracy in the determination of the integrated ESR intensities. Considering the observed similarities of the shape of the ESR signals and of the $I_{ESR}(T)$ dependences normalized per $\{Cu_3(3,4\text{-bopb})(pmdta)_2\}^{2+}$ unit, one can conclude that the ESR response of **10c**–**f** is given basically by the arithmetical sum of the individual units comprising the respective molecule. Thus, no evident signatures of a magnetic interaction between the endgrafted $\{Cu_3(3,4\text{-bopb})(pmdta)_2\}^{2+}$ units within the dendrimers could be observed and hence no dendritic effects.

Magnetic properties: The *J* values of **10c**–**f** are practically identical for all samples besides the somewhat larger value for **10d,** which is, however, still within the 5 % of the uncertainly of the fit. Furthermore, the obtained magnetic exchange constants are close to those of other

discrete trinuclear Cu^{II} bis(oxamato) species with tridentate amines as terminal ligands.[70,103,104] This observation is consistently with the conclusion on the isolated character of the $\{Cu_3(3,4\text{-bopb})(pmdta)_2\}^{2+}$ units in the studied dendrimers and hence no dendritic effects with respect to the magnetic properties of **10c**–**f** could be observed.

To verify this further, magnetisation measurements *vs* magnetic field *M*(*H*) of **10c**–**f** at T = 1.8 K were performed, cf. Figure 11. To enable a comparison, the data are normalised to the *M* value of the respective complex at a field of 7 T where the magnetisation is practically saturated. The curves are almost indistinguishable in this representation. As exemplified in the inset in Figure 11, all curves can be very well fitted with the Brillouin function with S = ½. Indeed, at low temperatures and due to a strong exchange interaction $J \sim 112$ cm^{-1} between three Cu^{II} spins S = ½ only the spin – ½ doublet ground state is populated and contributes to the magnetisation. The success of the fitting of all M(H) curves using the spin value S = ½ gives one more evidence for the absence of the magnetic interaction of the trinuclear Cu^{II} bis(oxamato) units in the studied samples.

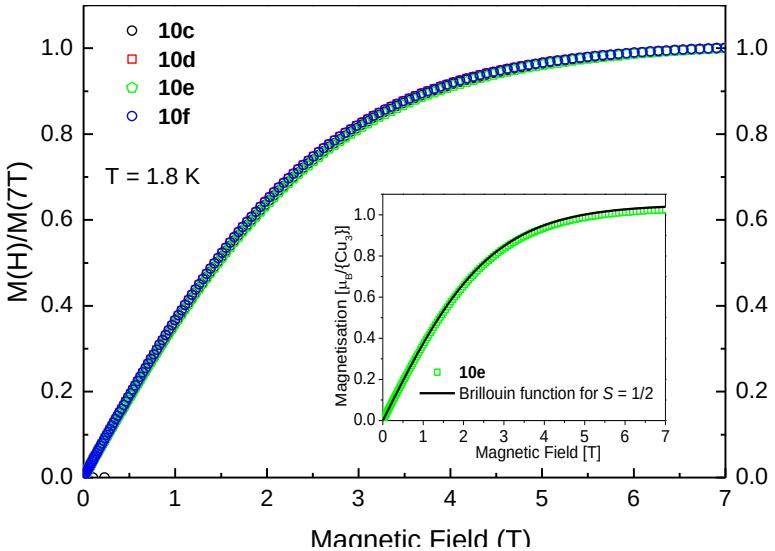

Figure 11. Magnetisation *vs* magnetic field *M*(*H*) of **10c–f** at T = 1.8 K normalized to its respective value at $\mu_0 H$ = 7 T. Inset illustrates the fit of *M*(*H*) to the Brillouin function with S = ½ on example of **10e**. The saturation magnetisation $M_s = 1.02\mu_B$ is very close to the expected value $M_s = g \cdot S\mu_B$ for S = ½ and g = 2.1 (see Table 2).

Conclusion

Dendrimers, carrying two (**9c**/**10c**), three (**9d**/**10d**), five (**9e**/**10e**) or ten (**9f**/**10f**) endgrafted $\{M(3,4\text{-bopbO})\}^{2-}/\{Cu_3(3,4\text{-bopb})(pmdta)_2\}^{2+}$ complex fragments could be successfully synthesised and their identities could be determined unambiguously. Reaction conditions for the synthesis of precursors of **10c**–**f** were optimised first and revealed that the peptide

coupling reaction of corresponding $-NH_2$ endgrafted PAMAN dendrimers with the acyl fluoride 3,4-bopbH_2EtF (**8**) is suited best to achieve the dendrimers in reasonable yield and pure state. Instead, trials to convert the carbon acid 3,4-bopbH_2Et_2OH (**1**) to transition metal complexes gave astonishingly rapidly rise to the formation of symmetric methylene diester in form of binuclear $[Bu_4N]_4[\{M(3,4\text{-bopbO})\}_2CH_2]$ (**M-3**, M = Cu, Ni). Both the **M-3** complexes and $[Bu_4N]_3[Ni(3,4\text{-bopbO})]$ (**4**), respectively, are inappropriate to be bonded to $-NH_2$ endgrafted PAMAN dendrimers. As **7f** could not be obtained free of **8** and hence not analytically pure, we abstained from the synthesis of higher generation dendrimers. Thus, we regard with respect to the delivery of pure materials the dendrimers **9f** and **10f** as the core generation of this series, as long as the here reported synthetic approach is applied.

The electronic absorption spectra of **9b–f** and **10c–f** as well as the ESR and magnetic properties of **10c–f** were studied. All compounds show typically features of mononuclear $\{Cu(3,4\text{-bopb})\}^{2-}$ (**9b–f**) and trinuclear $\{Cu_3(3,4\text{-bopb})(pmdta)_2\}^{2-}$ (**10c–f**) entities in a linear accordance to the number of complex fragments per molecule and hence no dendritic effects could be observed. However, as the $\{Cu_3(3,4\text{-bopb})(pmdta)_2\}^{2+}$ endgrafted complex fragments exhibit magnetic exchange interaction, dendrimers **10c**–**f** can be assigned as "magneto dendrimers".

Experimental Section

General methods and materials

All reactions were carried out under an argon atmosphere using standard Schlenk techniques. Used solvents and liquid compounds were purified according to standard procedures.[105] Unless stated otherwise, *cf.* below, all further chemicals were purchased from commercial sources and used as received without further purification. 3,4-bopbH_2Et_2OH (**1**),[43] $N(CH_2CH_2C(O)NHCH_2CH_2NH_2)_3$ (**5d**), $H_2NCH_2CH_2HN(O)CCH_2CH_2N(CH_2CH_2N[CH_2CH_2C(O)NHCH_2CH_2NH_2]_2)_2$ (**5e**) and $(H_2NCH_2CH_2HN(O)CCH_2CH_2)_2NCH_2CH_2HN(O)CCH_2CH_2N(CH_2CH_2N\{CH_2CH_2C(O)NHCH_2CH_2N[CH_2CH_2C(O)NHCH_2CH_2NH_2]_2\}_2)_2$ (**5f**)[81,82] were prepared according to published procedures. Figure S2† gives IR spectra and Figures S13–S27† give the ^1H, $^{13}C\{^1H\}$ and $^1H,^1H$-COSYGPSW, $^1H,^{13}C$-HMBCGP and HSQCETGP NMR spectra of **5d–f**. $[Cu(pmdta)(BF_4)_2]$ (**2d**) was synthesised by the reaction of $[Cu(BF_4)_2(H_2O)_6]$ and pmdta (*N*,*N*,*N'*,*N''*,*N''*-pentamethyldiethylenetriamine) in MeOH.[106] Anhydrous $NiCl_2$ (**2c**) was obtained by refluxing $NiCl_2{\cdot}6H_2O$ (**2b**) in thionyl chloride, followed by removal of residual thionyl chloride in vacuum.

Instruments

NMR spectra were recorded with a Bruker Avance III 500 UltraShield spectrometer (500.3 MHz for ^{1}H, 125.8 MHz for ^{13}C{^{1}H}) in the Fourier transform mode. Chemical shifts are reported in δ (parts per million) downfield from tetramethylsilane with the solvent as reference signal (^{1}H NMR: $CDCl_3$, δ = 7.26 ppm; DMSO-d_6, δ = 2.50 ppm; ^{13}C{^{1}H} NMR: $CDCl_3$, δ = 77.16 ppm; DMSO-d_6 δ = 39.52 ppm). Elemental analyses were performed with a Thermo FlashAE 1112 instrument. High-resolution mass spectra were recorded with a Bruker Daltonik micrOTOF-QII spectrometer. FT-IR spectra were recorded with a Nicolet IR 200 spectrometer (Fa. Thermo) as KBr pellets or between NaCl plates. High-resolution mass spectra were recorded with a Bruker Daltonik microTOF-QII spectrometer. UV/Vis solution spectra were measured at ambient temperature with a Genesys 6 spectrophotometer. The labelling scheme used for the assignment of individual NMR characterised compounds is summarised in Figures S8–S10.† The powder ESR spectra of **10c–f** were recorded with a Bruker EMX spectrometer operating in the X-band with a modulation frequency of 100 kHz. Handling of ESR spectra was carried out using Win-EPR® computer programs,[107] spectral simulations were performed with Simfonia program.[108] Static magnetic susceptibility of **10c**–**f** was measured with a 7 T VSM-SQUID magnetometer from Quantum Design at a field of 1 Tesla in a temperature range 2–300 K.

X-ray crystallography

Intensity data for **Cu-3** and **Ni-3** were collected with an Oxford Gemini S diffractometer at 100 K with Cu Kα radiation (λ = 1.54184 Å). The structures were solved by direct methods and refined by full-matrix least-squares procedures on F^2.[109] All non-hydrogen atoms were refined anisotropically, and a riding model was employed in the treatment of the hydrogen atom positions. The atoms C74, C75 (0.52/0.48) of **Cu-3** and C49–C51 (0.52/0.48) of **Ni-3** are disordered and were refined to split occupancies given in brackets. For both **Cu-3** and **Ni-3** the MeCN packing solvent molecule with the atoms C90, C91, N10 was refined partially occupied with an occupancy of 0.5.

Synthesis of $[Bu_4N]_4[\{M(3,4\text{-bopbO})\}_2CH_2]$ (M = Cu, Cu-3; M = Ni, Ni-3). To a suspension of **1** (400 mg, 1.14 mmol) in EtOH (50 mL) was added drop-wise a solution of $[Bu_4N]OH$ (3.86 g, 5.68 mmol, 40 % in H_2O) in water (25 mL) under aerobic conditions. The solution was heated at reflux for 30 min. After cooling to ambient temperature an aqueous solution (25 mL) of **2a** (194 mg, 1.14 mmol) or **2b** (271 mg, 1.14 mmol) was added drop-wise

and stirring was continued for 1 h. After extraction of the reaction mixture with CH_2Cl_2 (3 × 50 mL), the organic phase was extracted with water (2 × 50 mL). After drying the organic phase with Na_2SO_4 and reducing the solvent to 5 mL, solids of **Cu-3** or **Ni-3** were precipitated by addition of thf (5 mL) and Et_2O (50 mL). The violet (**Cu-3**) or orange (**Ni-3**) coloured solid was washed with Et_2O (3 × 10 mL) and dried in vacuum. Yield of **Cu-3**: 550 mg (0.32 mmol, 56 % based on **1**). Yield of **Ni-3**: 485 mg (0.29 mmol, 51 % based on **1**).

Cu-3: Anal. Calcd for $C_{87}H_{152}N_8O_{16}Cu_2{\cdot}H_2O$ (1711.29): C, 61.06; H, 9.07; N, 6.55 %. Found: C, 61.20; H, 9.23; N, 6.62 %. IR (KBr): $\tilde{\upsilon}$ [cm^{-1}] 3422 (w, br), 2962 (s), 2931 (m, sh), 2875 (m), 1720 (m), 1678 (s), 1650 (s), 1623 (vs), 1570 (m), 1483 (m), 1438 (m), 1397 (m), 1285 (m), 1224 (w), 1182 (w), 1156 (w), 1107 (w), 1050 (w), 991 (m). UV/Vis (MeCN): λ_{max} [nm] (ε [l mol^{-1} cm^{-1}]) 212 (41624), ca. 243 (sh) (27356), 283 (37264), 292 (38492), 337 (sh) (24284), 356 (27748), 564 (393).

Ni-3: Anal. Calcd for $C_{87}H_{152}N_8O_{16}Ni_2{\cdot}H_2O$ (1701.58): C, 61.41; H, 9.12; N, 6.59 %. Found: C, 61.47; H, 9.30; N, 6.78 %. ^{1}H NMR (DMSO-d_6): δ 0.94 (t, $^3J_{H,H}$ = 7.2 Hz, 48H, [(C*H*$_3$CH$_2$CH$_2$CH$_2$)$_3$N]$^+$), 1.31 (qt, $^3J_{H,H}$ = 7.2 Hz, $^3J_{H,H}$ = 7.2 Hz, 32H, [(CH$_3$C*H*$_2$CH$_2$CH$_2$)$_3$N]$^+$), 1.57 (tt, $^3J_{H,H}$ = 8.3 Hz, $^3J_{H,H}$ = 7.2 Hz, 32H, [(CH$_3$CH$_2$C*H*$_2$CH$_2$)$_3$N]$^+$), 3.16 (t, $^3J_{H,H}$ = 8.2 Hz, 32H, [(CH$_3$CH$_2$CH$_2$C*H*$_2$)$_3$N]$^+$), 6.04 (s, 2H, C*H*^{10}), 7.29 (dd, $^3J_{H,H}$ = 8.4, Hz, $^4J_{H,H}$ = 2.1 Hz, 2H, C*H*^{7}), 7.85 (d, $^3J_{H,H}$ = 8.4 Hz, 2H, C*H*^{8}), 8.42 (d, $^4J_{H,H}$ = 2.1 Hz, 1H, C*H*^{5}). ^{13}C{^{1}H} NMR (DMSO-d_6): δ 13.5 ([(*C*H$_3$CH$_2$CH$_2$CH$_2$)$_3$N]$^+$), 19.2 ([(CH$_3$*C*H$_2$CH$_2$CH$_2$)$_3$N]$^+$), 23.1 ([(CH$_3$CH$_2$*C*H$_2$CH$_2$)$_3$N]$^+$), 57.6 ([(CH$_3$CH$_2$CH$_2$*C*H$_2$)$_3$N]$^+$), 79.6 (O*C*H$_2$O), 117.3/119.0/120.1/123.7/143.1/148.3 (*C*^{Ph}), 161.3/161.9 (*C*$^{2,2'}$), 164.7 (*C*^{9}), 169.0/169.5 (*C*H$^{1,1'}$). IR (KBr): $\tilde{\upsilon}$ [cm^{-1}] 3435 (m, br), 2962 (s), 2931 (m, sh), 2874 (m), 1722 (m), 1670 (s), 1652 (s), 1631 (vs), 1573 (m), 1486 (m), 1440 (m), 1400 (m), 1283 (m), 1224 (w), 1181 (w), 1154 (w), 1106 (w), 1050 (w), 997 (m). UV/Vis (MeCN): λ_{max} [nm] (ε [l mol^{-1} cm^{-1}]) 259 (44636), ca. 287 (sh) (25928), ca. 316 (sh) (14716). Figure S1† gives IR spectra of **Cu-3** and **Ni-3**. Crystals suitable for X-ray crystallographic studies were grown by slow diffusion of Et_2O into MeCN solutions of **Cu-3** and **Ni-3**.

Synthesis of [Bu$_4$N]$_3$[Ni(3,4-bopbO)] (4). To a suspension of **1** (400 mg, 1.14 mmol) in MeOH (50 mL) was added drop-wise a solution of [Bu$_4$N]OH (3.24 g, 5 mmol, 40 % in MeOH) in MeOH (25 mL). The solution was heated at reflux for 30 min. After cooling to ambient temperature a solution of **2c** (238 mg, 1 mmol) in MeOH (20 mL) was added drop-wise and stirring was continued for 1 h. The reaction solution was evaporated to dryness in

vacuum and the residue was dissolved in MeCN (20 mL). Afterwards, Et_2O (10 mL) was added and the obtained solid was removed. From the supernatant solution complex **4** could be precipitated by addition of thf (5 mL) and Et_2O (50 mL). The precipitated orange coloured solid was filtered off, washed with Et_2O (3 × 10 mL) and dried in vacuum. Yield: 560 mg (0.32 mmol, 52 % based on **1**). Due to the very hygroscopic nature of **4** no elemental analysis was measured.

4: ^{1}H NMR (DMSO-d_6): δ 0.94 (t, $^3J_{H,H}$ = 7.3 Hz, 36H, [(CH_3CH$_2$CH$_2$CH$_2$)$_3$N]$^+$), 1.32 (qt, $^3J_{H,H}$ = 7.3 Hz, $^3J_{H,H}$ = 7.3 Hz, 24H, [(CH$_3$CH_2CH$_2$CH$_2$)$_3$N]$^+$), 1.54–1.61 (m, 24H, [(CH$_3$CH$_2$CH_2CH$_2$)$_3$N]$^+$), 3.15–3.20 (m, 24H, [(CH$_3$CH$_2$CH$_2$CH_2)$_3$N]$^+$), 7.10 (dd, $^3J_{H,H}$ = 8.1 Hz, $^4J_{H,H}$ = 1.7 Hz, 1H, CH^7), 7.63 (d, $^3J_{H,H}$ = 8.1 Hz, 1H, CH^8), 8.24 (d, $^4J_{H,H}$ = 1.7 Hz, 1H, CH^5). ^{13}C{^{1}H} NMR (DMSO-d_6): δ 13.4 ([(*C*H$_3$CH$_2$CH$_2$CH$_2$)$_3$N]$^+$), 19.1 ([(CH$_3$*C*H$_2$CH$_2$CH$_2$)$_3$N]$^+$), 23.1 ([(CH$_3$CH$_2$*C*H$_2$CH$_2$)$_3$N]$^+$), 57.5 ([(CH$_3$CH$_2$CH$_2$*C*H$_2$)$_3$N]$^+$), 116.2/119.9/122.6/135.1/141.9/143.0 (C^{Ph}), 160.3/160.6 ($C^{2,2'}$), 168.9 (C^9), 170.1/170.4 ($C^{1,1'}$).

Synthesis of [RNH$_3$][tdqc] (6a, R = Me; 6b, R = Pr). To a suspension of **1** (176 mg, 0.5 mmol) in MeOH (25 mL) **5a** (124 mg, 4 mmol) or **5b** (236 mg, 4 mmol) in MeOH (25 mL) was drop-wise added. After stirring for 1 h at ambient temperature the reaction solution was reduced to 10 mL and stored over night at 7 °C. The precipitated colourless solid of **6a** and **6b** were filtered off, washed with cold MeOH (2 × 10 mL) and dried in air. Yield of **6a**: 107 mg (0.45 mmol 90 % based on **1**). Yield of **6b**: 114 mg (0.43 mmol, 86 % based on **1**).

6a*:* Anal. Calcd for $C_{10}H_{11}N_3O{\cdot}H_2O$ (255.23): C, 47.06; H, 5.13; N, 16.46 %. Found: C, 46.84; H, 5.23; N, 16.28 %. IR (KBr): $\tilde{\upsilon}$ [cm^{-1}] 3423–2826 (br, m), 1700 (s), 1676 (vs), 1625 (m), 1572 (s), 1410 (vs), 830 (w), 780 (w), 660 (w). ^{1}H NMR (DMSO-d_6): δ 2.38 (s, 3H, [CH_3NH$_3$]$^+$), 3.45 (bs, 3H, [CH$_3$NH_3]$^+$), 7.06 (d, $^3J_{H,H}$ = 8.2 Hz, 1H, CH^8), 7.61 (dd, $^4J_{H,H}$ = 1.5 Hz, $^3J_{H,H}$ = 8.2 Hz, 1H, CH^7), 7.73 (d, $^4J_{H,H}$ = 1.5 Hz, 1H, CH^5), 9.36 (bs, 2H, N$H^{10,11}$ N*H*). ^{13}C{^{1}H} NMR (DMSO-d_6): δ 24.5 ([*C*H$_3$NH$_3$]$^+$), 114.0/116.2/124.1/124.7/126.6/ 133.7 (C^{Ph}), 155.2/155.3 ($C^{1,2}$), 168.7 (C^9).

6b: Anal. Calcd for $C_{12}H_{15}N_3O_4{\cdot}H_2O$ (283.28): C, 50.88; H, 6.05; N, 14.83 %. Found: C, 50.79; H, 6.00; N, 14.80 %. ^{1}H NMR (DMSO-d_6): δ 0.89 (t, $^3J_{H,H}$ = 7.4 Hz, 3H, [CH_3CH$_2$CH$_2$NH$_3$]$^+$), 1.53 (tq, $^3J_{H,H}$ = 7.4 Hz, $^3J_{H,H}$ = 7.4 Hz, 2H, [CH$_3$CH_2CH$_2$NH$_3$]$^+$), 2.70 (t, $^3J_{H,H}$ = 7.4 Hz, 2H, [CH$_3$CH$_2$CH_2NH$_3$]$^+$), 3.37 (bs, 3H, [CH$_3$CH$_2$CH_2NH_3]$^+$), 7.05 (d, $^3J_{H,H}$ = 8.2 Hz, 1H, CH^8), 7.60 (dd, $^4J_{H,H}$ = 1.5 Hz, $^3J_{H,H}$ = 8.2 Hz, 1H, CH^7), 7.71 (d, $^4J_{H,H}$ = 1.5 Hz, 1H, CH^5), 9.40 (bs, 2H, N$H^{10,11}$). ^{13}C{^{1}H} NMR (DMSO-d_6): δ 11.0

([*C*H$_3$CH$_2$CH$_2$NH$_3$]$^+$), 21.5 ([CH$_3$*C*H$_2$CH$_2$NH$_3$]$^+$), 40.7 ([CH$_3$CH$_2$*C*H$_2$NH$_3$]$^+$), 114.0/116.2/124.1/124.7/126.6/133.7 (*C*^{Ph}), 155.2/155.3 (*C*^{1,2}), 168.4 (*C*^{9}). IR (KBr): $\tilde{\nu}$ [cm^{-1}] 3340–2764 (br, m), 1683 (s), 1623 (w), 1603 (w), 1536 (m), 1508 (m), 1394 (s), 1281 (w), 777 (w). Figure S3† displays IR spectra of **6a** and **6b**.

Synthesis of [(H$_2$NCH$_2$CH$_2$HN(O)CCH$_2$CH$_2$)$_2$NCH$_2$CH$_2$HN(O)CCH$_2$CH$_2$N[CH$_2$CH$_2$N-(CH$_2$CH$_2$C(O)NH-CH$_2$CH$_2$N{CH$_2$CH$_2$C(O)NHCH$_2$CH$_2$NH$_2$}$_2$)$_2$]$_2$ (den^{X}H$_{10}$, 5f). 5f was prepared by a divergent consecutive synthesis procedure starting from compound **5e**.[81] To a solution of **5e** (2.63 g, 3.9 mmol) in MeOH methyl acrylate (6.72 g, 78 mmol) was added in a single portion. After stirring for 5 d at ambient temperature all volatiles were removed under vacuum by oil-pump vacuum. Afterwards, an excess of ethylene diamine (27.1 g, 200 mmol) was added in a single portion. The reaction mixture was again stirred for 5 d. For purification all volatiles were evaporated by applying oil-pump vacuum at 40–50 °C. **5f** was obtained as colourless and highly viscous oil. Yield: 6.87 g (97 % based on **5e**).

5f: Anal. Calcd for C$_{79}$H$_{163}$N$_{38}$O$_{15}$ (1815.35): C, 52.27; H, 9.05; N, 25.46 %. Found: C, 51.66; H, 9.29%; N, 25.56 %. Although, these results are outside the range viewed as establishing analytical purity, they are provided to illustrate the best values obtained to date. ^{1}H NMR (CDCl$_3$): δ 1.51 (s, 20H, N*H*^{1}), 2.22–2.36 (m, 30H, C*H*^{6,7,12,13}), 2.40–2.54 (m, 18 H, C*H*^{8,14,15}), 2.60–2.73 (m, 30H, C*H*^{6,7,12,13}), 2.73–2.86 (m, 20H, C*H*^{2}), 3.11–3.31 (m, 30H, C*H*^{3,9}), 7.45–8.17 (m, 15H, N*H*^{4,10}). ^{13}C{^{1}H} NMR (CDCl$_3$): δ 34.3/34.5 (*C*H^{6,7,12,13}), 37.9 (*C*H^9), 41.7 (*C*H^2), 42.4/42.5 (*C*H^3), 50.6/50.7 (*C*H^{6,7,12,13}), 51.5 (*C*H^8), 52.2/52.9 (*C*H^{14,15}), 170.9 (*C*^{5,11}). IR (NaCl): $\tilde{\nu}$ [cm^{-1}] 3281 (s, br), 3086 (m), 2936 (m), 2862 (m), 2833 (m), 1645 (s), 1554 (s), 1462 (m), 1434 (m), 1356 (m), 1285 (m), 1256 (m), 1127 (w), 1038 (w), 946 (w). Figure S2† displays the IR spectrum and Figures S23-S27† display the NMR spectra of **5f**.

Synthesis of 3,4-bopbH$_2$Et$_2$F (8).

Method 1: To a suspension of **1** (1.762 g, 5 mmol) in CH$_2$Cl$_2$ (150 mL), pyridine (791 mg, 10 mmol) and cyanurfluoride (1.36 g, 10 mmol) was added in a single portion and the thus obtained reaction mixture was stirred for 4 h at 0°. After addition of a mixture of ice/water (ratio 1:1 (*v*/*v*), 100 g) the obtained solid was removed by filtration. The organic phase was washed with cold water (3 × 50 mL), dried with Na$_2$SO$_4$ and concentrated to 5 mL. Compound **8** was precipitated by addition of Et$_2$O (100 mL), filtered off and washed with

Et_2O (3 × 10 mL). The colourless product was dried in vacuum. Yield: 1.28 g (3.61 mmol, 72 % based on **1**).

Method 2: To a solution of *N,N'*-dicyclohexylcarbodiimide (1.87 g, 9.04 mmol) and $(HF)_x$·pyridine (284 mg, 9.94 mmol, 0.26 mL, 70 % HF) in CH_2Cl_2 (50 mL) a suspension of **1** (3.186 g, 9.04 mmol) and pyridine (2 mL) in CH_2Cl_2 (50 mL) was added drop-wise. After stirring for 4 h, the mixture was filtered. The filtrate was extracted with an aqueous HCl solution (0.02 %, 3 × 50 mL), dried with Na_2SO_4 and reduced in vacuum to dryness. After washing the solid with thf (3 × 20 mL), the filtrate was reduced to 5 mL. The colourless product was precipitated by addition of Et_2O (30 mL), filtered and dried in air. Yield: 2.67 g (7.53 mmol, 83 % based on **1**).

8: Anal. Calcd for $C_{15}H_{15}FN_2O_7$ (354.29): C, 50.85; H, 4.27; N, 7.91 %. Found: C, 51.00; H, 4.26; N, 7.60 %. IR (KBr): $\tilde{\upsilon}$ [cm^{-1}] 3301 (vs), 3075 (w), 2985 (w), 2945 (w), 2910 (w), 1812 (s, C(O)F), 1767 (m), 1739 (m), 1710 (s) 1688 (s), 1527 (m), 1480 (m) 1307 (m), 1173 (m). ^{1}H NMR (DMSO-d_6): δ 1.34/1.33 (t/t, $^3J_{H,H}$ = 7.1 Hz, 6H, C$H^{1,1'}$), 4.34/4.33 (q/q, $^3J_{H,H}$ = 7.1 Hz, 4H, C$H^{2,2'}$), 7.97 (m, 2H, C$H^{10,11}$), 8.21 (s, 1H, CH^8), 10.62 (s, 1H, NH^5), 10.66 (s, 1H, N$H^{5'}$). ^{13}C{^{1}H} NMR (DMSO-d_6): δ 13.78 (*C*H$^{1,1'}$), 62.65 (*C*H$^{2,2'}$), 121.0 (d, $^2J_{C,F}$ = 63 Hz, *C*^{9}), 125.4 (CH^{11}), 129.2 (d, $^3J_{C,F}$ = 27 Hz, *C*H^8), 129.4 (d, $^3J_{C,F}$ = 33 Hz, *C*H^{10}), 136.8 (*C*^{7}), 155.7/156.0 (*C*$^{2,2'}$), 156.1 (d, $^1J_{C,F}$ = 342 Hz, *C*^{12}), 159.9/159.9 (*C*$^{1,1'}$). Figure S3† displays the IR spectrum and Figures S28 and 29† display the NMR spectra of **8**.

Synthesis of 3,4-bopbH_2Et$_2$NPrH (7b). To **8** (354 mg, 1 mmol) in CH_2Cl_2 (20 mL) a solution of **5b** (59 mg, 1 mmol) and pyridine (79 mg, 1 mmol) in CH_2Cl_2 (20 mL) was added drop-wise. After stirring this reaction mixture for 12 h at ambient temperature the resulting yellow suspension was evaporated to dryness. A saturated solution of $NaHCO_3$ (15 mL) was added and the mixture was stirred for 15 min. The obtained solid of **7b** was filtered, washed with cold water (2 × 5 mL) and Et_2O (3 × 10 mL) and dried in vacuum. Yield: 330 mg (0.84 mmol, 84 % based on **8**).

7b: Anal. Calcd for $C_{18}H_{23}N_3O_7$ (393.39): C, 54.96; H, 5.89; N, 10.68 %. Found: C, 54.99; H, 5.91; N, 10.63 %. IR (KBr): $\tilde{\upsilon}$ [cm^{-1}] 3387 (m), 3315 (w), 2971 (w), 2938 (w), 2868 (w), 1765 (vs), 1732 (s), 1717 (s), 1696 (s), 1654 (s), 1543 (s), 1526 (vs), 1487 (m), 1297 (s), 1262 (s), 1182 (s), 1018 (m), 664 (w). ^{1}H NMR (DMSO-d_6): δ 0.9 (t, $^3J_{H,H}$ = 7.3 Hz, 3H, CH^{16}), 1.32/1.33 (t, $^3J_{H,H}$ = 7.1 Hz, 6H, C$H^{1,1'}$), 1.54 (sextet, $^3J_{H,H}$ = 7.3 Hz, $^3J_{H,H}$ = 7.3 Hz, $^3J_{H,H}$ = 7.3 Hz, 2H, CH^{15}), 3.23 (td, $^3J_{H,H}$ = 5.5 Hz, $^3J_{H,H}$ = 7.3 Hz, 2H, CH^{14}), 4.29–4.36 (M, 4H, C$H^{2,2'}$), 7.72 (d, $^3J_{H,H}$ = 8.5 Hz, 1H, CH^{11}), 7.78 (dd, $^3J_{H,H}$ = 8.5 Hz, $^4J_{H,H}$ = 2 Hz, 1H,

C*H*[10]), 8.02 (d, $^4J_{H,H}$ = 2 Hz, 1H, C*H*[8]), 8.49 (t, $^3J_{H,H}$ = 5.5 Hz, 1H, N*H*[13]), 10.42/10.54 (s/s, 2H, N*H* [5,5']). $^{13}C\{^1H\}$ NMR (DMSO-d_6): δ 11.4 (*C*H[16]), 13.8/13.8 (*C*H[1,1']), 22.3 (*C*H[15]), 41.0 (*C*H[14]), 62.5/62.6 (*C*H[2,2']), 124.7/125.1/125.3/129.0/132.3/132.4 (*C*[Ph]), 155.6/155.8 (*C*[4,4']), 160.1/160.1 (*C*[3,3']), 164.9 (*C*[12]). Figure S4† displays IR spectrum of **7b**.

Synthesis of en^{II}(3,4-bopbH$_2$Et$_2$)$_2$ (7c). 8 (359 mg, 1.01mmol) was reacted with **5c** (304 mg, 0.50 mmol) and pyridine (79 mg, 1.01 mmol) under the same reaction conditions as described for **7b**. After stirring for 2 d and appropriate work-up as described for **7b**, compound **7c** could be isolated as colourless solid. Yield: 321 mg (0.44 mmol, 87 % based on **8**).

7c: Anal. Calcd for $C_{32}H_{36}N_6O_{14}$ (728.66): C, 52.75; H, 4.98; N, 11.53 %. Found: C, 52.80; H, 5.00; N, 11.21 %. ^{1}H NMR (DMSO-d_6): δ 1.32/1.33 (t, $^3J_{H,H}$ = 7.1 Hz, 12H, C*H*[1,1']), 3.45 (s, 4H, C*H*[14]), 4.28–4.36 (m, 8H, *C*H[2,2']), 7.74 (d, $^3J_{H,H}$ = 8.4 Hz, 2H, *C*H[11]), 7.80 (dd, $^3J_{H,H}$ = 8.5 Hz, $^4J_{H,H}$ = 2 Hz, 2H, *C*H[10]), 8.05 (s, 2H, *C*H[8]), 8.66 (s, 2H, N*H*[13]), 10.42/10.54 (s/s, 4H, N*H*[5,5']). $^{13}C\{^1H\}$ NMR (DMSO-d_6): δ 13.8/13.8 (*C*H[1,1']), 62.6/62.6 (*C*H[2,2']), ca. 39.5 (*C*H[14]), 124.7/125.2 (*C*H[10,11]), 125.4 (*C*H[8]), 129.1 (*C*[6]), 132.1(*C*[9]), 132.6 (*C*[7]), 155.6/155.9 (*C*[4,4']), 160.1/160.14 (*C*[3,3']), 165.3 (*C*[12]). IR (KBr): $\tilde{\nu}$ [cm^{-1}] 3311 (s), 3254 (s), 2989 (w), 2962 (w), 2941 (w), 2903 (w), 2876 (w), 1170 (s), 1740 (s), 1723 (s), 1689 (s), 1644 (s), 1592 (m), 1546 (s), 1532 (s), 1485 (s), 1413 (m), 137 (s), 1300 (s), 1225 (s), 1177 (s), 1107 (m), 1016 (s), 950 (m), 898 (m), 855 (m), 837 (m), 770 (m). MS (ESI-TOF, positive, CH_2Cl_2/MeCN): *m/z* = 729.2362 [**7c** + H]$^+$ (22 %); 751.2182 [**7c** + Na]$^+$ (100 %); 767.1921 [**7c** + K]$^+$ (10 %). Figure S5† displays IR spectrum, Figures S30–S33† display NMR Spectra, Figure S49† displays ESI-MS spectrum of **7c**.

Synthesis of den^{III}(3,4-bopbH$_2$Et$_2$)$_3$ (7d). 8 (1.35 g, 3.82 mmol) was reacted with **5d** (416 mg, 1.16 mmol) and pyridine (330 mg, 4.17 mmol) under the same reaction conditions as described for **7b**. After stirring for 2 d, compound **7d** was filtered off, washed excessively with Et_2O (5 × 15 mL) and thf (5 × 15 mL) and was dried in vacuum. Yield: 1.28 g (0.54 mmol, 73% based on **8**).

7d: Anal. Calcd for $C_{60}H_{75}N_{13}O_{24}$ (1362.31): C, 52.90; H, 5.55; N, 13.37 %. Found: C, 52.51; H, 5.68; N, 13.22 %. ^{1}H NMR (DMSO-d_6) : δ 1.31/1.31 (t/t, $^3J_{H,H}$ = 7.1 Hz, 18H, C*H*[1,1']), 2.16–2.30/2.62–2.73 (m/m, 12H, C*H*[18,19]), 3.13–3.25/3.25–3.36 (m/m, 12H, C*H*[14,15]), 4.27–4.34 (m, 12H, C*H*[2,2']), 7.72 (d, $^3J_{H,H}$ = 8.5 Hz, 3H, C*H*[11]), 7.77 (dd, 3H, $^3J_{H,H}$ = 8.5 Hz, $^4J_{H,H}$ = 1.9 Hz, C*H*[10]), 8.02 (m, 5H, C*H*[8]/N*H*[16]), 8.58 (t, 3H, $^3J_{H,H}$ = 5.3 Hz, N*H*[13]), 10.50 (s, 6H, N*H*[5,5']). $^{13}C\{^1H\}$ NMR (DMSO-d_6): δ 13.8/13.9 (*C*H[1,1']), 33.38/49.07 (*C*H[18,19]), 38.2/ca.

39.6 (*C*H^{14,15})*, 62.6/62.7 (*C*H$^{2,2'}$), 124.8/125.2/125.5 (*C*H^{8,10,11}), 129.1 (*C*^{6}), 132.1/132.6 (*C*^{9,7}), 155.6/155.9 (*C*$^{4,4'}$), 160.2 (*C*$^{3,3'}$), 165.2 (*C*^{12}), 171.5 (*C*^{17}). IR (KBr): $\tilde{\nu}$ [cm^{-1}] 3309 (vs, br), 3091 (m, br), 2984 (m), 2934 (m), 2850 (m), 1741 (s), 1701 (vs), 1654 (vs), 1517 (vs), 1303 (s), 1215 (m), 1183 (s), 1112 (w), 1014 (m), 947 (w), 856 (w), 840 (w), 758 (w). MS (ESI-TOF, positive, CH_2Cl_2/MeCN): *m/z* = 471.3688 (100 %); 1362.5121 [**7d** + H]$^+$(3 %); 1384.4940 [**7d** + Na]$^+$ (1 %). Figure S5† displays IR spectrum, Figures S34–38† displays NMR Spectra, Figure S50† displays ESI-MS spectrum of **7d**.

Synthesis of den^{V}(3,4-bopbH$_2$Et$_2$)$_5$ (7e). Compound **8** (451 mg, 1.26 mmol) was reacted with **5e** (162 mg, 0.24 mmol) and pyridine (90 mg, 0.1 mL, 1.26 mmol) under the same reaction conditions as described for **7b**. After stirring for 2 d and appropriate work-up (see **7d**), compound **7e** could be isolated as a colourless solid. Yield: 460 mg (0.20 mmol, 77 % based on **8**).

7e: Anal. Calcd for $C_{104}H_{133}N_{23}O_{40}$ (2345.30): C, 53.26; H, 5.72; N, 13.74 %. Found: C, 52.81; H, 5.43; N, 13.68 %. *Remark*: Despite prolonged drying of **7e** in vacuum at higher temperature (ca. 40 °C), the obtained material contained still smaller amounts of applied solvents. Such solvent contents could be detected by NMR spectroscopy (Figures S39 and S40†). It is assumed that these small solvent amounts are embedded within the macromolecule and thus alter the elemental analysis. Assuming that the composition of the isolated material corresponds to **7e·0.2CH$_2$Cl$_2$** the following calculated values would be obtained: C, 52.98; H, 5.69; N, 13.64 %; which compares well with the obtained values. ^{1}H NMR (DMSO-d_6): δ 1.29–1.34 (m, 30H, C*H*$^{1,1'}$); 2.16–2.27/2.60–2.75/3.15–3.26/3.26–3.40 (m, m, m, m, 10H/10H/10H/18H, C*H*^{14,15,18,19,20,21}), 4.28–4.35 (m, 20H, C*H*$^{2,2'}$), 7.72 (d, 5H, $^3J_{H,H}$ = 8.5 Hz, C*H*^{11}), 7.76 (dd, 5H, $^4J_{H,H}$ = 1.8 Hz, $^3J_{H,H}$ = 8.5 Hz, C*H*^{10}), 8.02 (d, 5H, $^4J_{H,H}$ = 1.5 Hz, C*H*^{8}), 8.05/8.85 (m/m, 10H, N*H*^{13,16}), 10.47 (s, 10 H, N*H*$^{5,5'}$). *Comment:* A more specific assignment of the hydrogen atoms C*H*^{14,15,18,19,20,21} to a specific ^{1}H NMR signal is not possible unambiguously. The C*H*^{20,21} atoms of **7e** might have a related chemical shift as those of **5e**, however, the DMSO-d_6 measurement of **7e** did not display such an individual signal. Instead, these atoms of **7e** might be superimposed by the NMR signal of C*H*^{14,15,18,19}, as indicated by additional 2D NMR experiments (Figures S41–43†). ^{13}C{^{1}H} NMR (DMSO-d_6): δ 13.8 (*C*H$^{1,1'}$), 31.2/37.9/39.1/49.2 (*C*H^{14,15,18,19,20,21}), 62.5/62.6 (*C*H$^{2,2'}$), 124.7/125.1/125.4 (*C*H^{8,10,11}), 129.0 (*C*^{6}), 132.0/132.5 (*C*^{7,9}), 155.6/155.8 (*C*$^{4,4'}$), 160.1 (*C*$^{3,3'}$), 165.2 (*C*^{12}), 171.6 3 (*C*H^{17}). IR (KBr): $\tilde{\nu}$ [cm^{-1}] 3281 (m, br), 3084 (m, br), 2984 (m), 2939 (m), 2875 (w), 2852

(w), 1756 (s), 1704 (vs), 1652 (vs), 1590 (m), 1525 (s), 1485 (m), 1371 (m), 1303 (vs), 1217 (m), 1184 (s), 1115 (w), 1015 (m), 948 (w), 857 (w), 752 (w). MS (ESI-TOF, positive, MeOH): *m/z* = 808.8526 [**7e** – 2(3,4-bopbH$_2$Et$_2$NHCH$_2$) + 2H]$^{2+}$ (54 %); 843.3269 (100 %); 948.8793 [**7e** – 3,4-bopbH$_2$Et$_2$NHCH$_2$COC$_4$H$_8$ + 2H]$^{2+}$ (45 %); 1173.4715 [**7e** + 2H]$^{2+}$ (96 %); 1616.7013 [**7e** – 2(3,4-bopbH$_2$Et$_2$NHCH$_2$) + H]$^{+}$ (46 %); 1981.8075 [2(**7e** – 3,4-bopbH$_2$Et$_2$O + H)]$^{2+}$; (8 %); 2345.9251 [**7e** + H]$^{+}$ (9 %). Figure S5† displays the IR spectrum, Figures S39–S43† displays the NMR spectra, Figures S51 and 52† display ESI-MS spectra of **7e**.

Synthesis of den^{X}(3,4-bopbH$_2$Et$_2$)$_{10}$ (7f). Compound **8** (734 mg, 2.07 mmol) was reacted with **5f** (365 mg, 0.20 mmol) and pyridine (169 mg, 2.13 mmol) under the same reaction conditions as described for **7b**. After stirring for 2 d and appropriate work-up (see **7d**), compound **7f** could be isolated as colourless solid. Yield: 913 mg (0.18 mmol, 86% based on **8**).

7f: Anal. Calcd for $C_{228}H_{301}N_{53}O_{85}$ (5155.10): C, 53.32; H, 5.92; N, 14.39 %. Found: Not performed, due to impurity of **8** as revealed by NMR characterisation. ^{1}H NMR (DMSO-d_6): δ 1.21–1.36 (m, 60H, C*H*$^{1,1'}$), 2.29–2.47/2.70–3.13/3.13–3.41 (m, 128H, C*H*^{14,15,18,19,20,21,24,25}), 4.23–4.36 (m, 40H, C*H*$^{2,2'}$), 7.68–7.88 (m, 20H, C*H*^{10,11}), 7.91–8.08 (m, 10H, C*H*^{8}), 8.08–8.39 (m, 20 H, N*H*^{13,16}), 8.58 (s, 5H, N*H*^{22}), 10.28–10.63 (m, 20H, N*H*$^{5,5'}$). ^{13}C{^{1}H} NMR (DMSO-d_6): δ 13.9 (*C*H$^{1,1'}$), 30.26/37.9/38.6/48.1/48.4 (*C*H^{14,15,18,19,20,21,24,25}), 62.7 (*C*H$^{2,2'}$), 124.9/125.1 (*C*H^{10,11}), 125.5 (*C*H^{8}), 129.1 (*C*^{6}), 132.1/132.6 (*C*^{7,9}), 155.7/155.9 (*C*$^{4,4'}$), 160.2 (*C*$^{3,3'}$), 165.3 (*C*^{12}), 170.9 (*C*^{17,23}). IR (KBr): $\tilde{\nu}$ [cm^{-1}] 3300 (m, br), 3255 (m, br), 3074 (m, br), 2986 (m), 2935 (w), 2902 (w), 2873 (w), 1813 (m), 1742 (s), 1710 (vs), 1650 (s), 1525 (s), 1482 (m), 1371 (m), 1305 (vs), 1216 (m), 1182 (s), 1115 (w), 1016 (m), 943 (w), 857 (w), 752 (w). MS (ESI-TOF, positive, H$_2$O/MeOH): *m/z* = 927.3635 (100 %); 1021.2137 [**7f** – C$_4$H$_8$ + 5H]$^{5+}$ (6 %); 1026.8200 [**7f** – C$_2$H$_4$ + 5H]$^{5+}$ (17 %); 1032.4263 [**7f** + 5H]$^{5+}$ (31 %); 1276.2685 [**7f** – C$_4$H$_8$ + 4H]$^{4+}$ (4 %); 1283.2763 [**7f** – C$_2$H$_4$ + 4H]$^{4+}$ (8 %); 1290.2841 [**7f** + 4H]$^{4+}$ (11 %); 1701.3514 [**7f** – C$_4$H$_8$ + 3H]$^{3+}$ (4 %); 1710.6993 [**7f** – C$_2$H$_4$ + 3H]$^{3+}$ (3 %); 1720.0431 [**7f** + 3H]$^{3+}$ (2 %). Figure S5† displays the IR spectrum, Figure S44–S48† displays NMR Spectra, Figure S53 and 54† displays ESI-MS spectra of **7f**.

Synthesis of [Bu$_4$N]$_2$[M(3,4-bopbNPrH)] (M = Cu, Cu-9b; M = Ni, Ni-9b). Compounds **Cu-9b** and **Ni-9b** were prepared according to the procedure described for **3a** and **3b**. To a suspension of **7b** (400 mg, 1.02 mmol) in EtOH (50 mL) a solution of [Bu$_4$N]OH (2.65 g,

4.07 mmol, 40% in H_2O) in water (25 mL) was added drop-wise. The solution was heated at reflux for 30 min. After cooling to ambient temperature an aqueous solution (20 mL) of **2a** (174 mg, 1.02 mmol) or **2b** (243 mg, 1.02 mmol) was added drop-wise and the thus obtain solution was stirred for 1 h. After extraction of the reaction mixture with CH_2Cl_2 (3 × 50 mL), the organic phase was again extracted with water (2 × 50 mL). After drying the organic phase with Na_2SO_4 and reducing the solvent to 5 mL, the solids of **Cu-9b** and **Ni-9b** were precipitated by addition of thf (5 mL) and Et_2O (50 mL). The violet (**Cu-9b**) or orange (**Ni-9b**) coloured solids were washed with Et_2O (3 × 20 mL) and dried in vacuum. Yield of **Cu-9b**: 679 mg (0.79 mmol, 77 % based on **7b**). Yield of **Ni-9b**: 635 mg (0.72 mmol, 71 % based on **7b**).

Cu-9b: Anal. Calcd for $C_{46}H_{83}N_5O_7Cu$ (881.73): C, 61.41; H, 9.52; N, 7.78 %. Found: C, 61.14 %; H, 9.69 %; N, 7.84 %. IR (KBr): $\tilde{\upsilon}$ [cm^{-1}] 3545 (br, w), 3364 (br, m), 3280 (br, m), 2962 (m), 2935 (m), 2875 (m), 1675 (m), 1640 (sh, s), 1630 (s), 1574 (s), 1550 (m), 1480 (m), 1427 (w), 1400 (m), 1322 (w), 1289 (m).UV/Vis (MeCN): λ_{max} [nm] (ε [l mol^{-1} cm^{-1}]) 212 (22214), 242 (14312), 278 (17310), 288 (16190), 338 (13108), 565 (214).

Ni-9b*:* Anal. Calcd for $C_{46}H_{83}N_5O_7Ni$ (876.87): C, 63.01; H, 9.54; N, 7.99 %. Found: C, 63.13 %; H, 9.60 %; N, 7.84 %. ^{1}H NMR (DMSO-d_6): δ 0.86 (t, $^3J_{H,H}$ = 7.3 Hz, 3H, CH^{16}), 0.94 (t, $^3J_{H,H}$ = 7.3 Hz, 24H, [CH_3CH$_2$CH$_2$CH$_2$N]$^+$), 1.32 (sextett, $^3J_{H,H}$ = 7.3 Hz, $^3J_{H,H}$ = 7.3 Hz, 16H, [CH$_3$CH_2CH$_2$CH$_2$N]$^+$), 1.49 (sextett, $^3J_{H,H}$ = 7.3 Hz, $^3J_{H,H}$ = 7.3 Hz, 2H, CH^{15}), 1.62-1.54 (m, 16H, [CH$_3$CH$_2$CH_2CH$_2$N]$^+$), 3.21–3.11 (m, 18H, [CH$_3$CH$_2$CH$_2$CH_2N]$^+$, CH^{14}), 7.08 (dd, $^3J_{H,H}$ = 8.5 Hz, $^4J_{H,H}$ = 1.6 Hz, 1H, CH^{10}), 7.78 (d, $^3J_{H,H}$ = 8.5 Hz, 1H, CH^{11}), 8.02 (t, $^3J_{H,H}$ = 5.5 Hz, 1H, NH^{13}), 8.25 (d, $^4J_{H,H}$ = 1.6 Hz, 1H, CH^8). ^{13}C{^{1}H} NMR (DMSO-d_6): δ 11.4 (CH^{16}), 13.5 ([CH$_3$CH$_2$CH$_2$CH$_2$N]$^+$), 19.2 ([CH$_3$$CH_2CH_2CH_2$N]$^+$), 22.5 ($CH^{15}$), 23.1 ([CH$_3CH_2$$CH_2CH_2$N]$^+$), 40.9 ($CH^{14}$), 57.5 ([CH$_3CH_2CH_2$$CH_2$N]$^+$), 116.9/117.5/120.2/127.5/ 142.3/145.4 (C^{Ph}), 161.3/161.0 ($C^{4,4'}$), 166.7 (C^{12}), 169.5/169.8 ($C^{3,3'}$). IR (KBr): $\tilde{\upsilon}$ [cm^{-1}] 3520–3290 (br, w), 2962 (m), 2933 (sh, m), 2875 (m), 1669 (s), 1640 (vs), 1580 (s), 1560 (m), 1483 (s), 1404 (m), 1290 (m), 880 (w). UV/Vis (MeCN): λ_{max} [nm] (ε [l mol^{-1} cm^{-1}]) 211 (22574), 256 (23892), ca. 279 (sh) (13866), ca. 307 (sh) (7012), 364 (8690), ca. 476 (sh) (245). Figure S4† displays the IR spectra of **Cu-9b** and **Ni-9b**.

Synthesis of [Bu$_4$N]$_4$[en^{II}{Cu(3,4-bopb)}$_2$] (9c). To a suspension of **7c** (771 mg, 1.06 mmol) in EtOH (100 mL) a solution of [Bu$_4$N]OH (5.56 g, 8.57 mmol, 40% in H_2O) in water (25 mL) was added drop-wise. This solution was heated at reflux for 30 min. After cooling to ambient temperature an aqueous solution of **2a** (370 mg, 2.16 mmol) was added drop-wise

and stirring was continued for 1 h. After extraction of the reaction mixture with CH_2Cl_2 (3 × 50 mL), the organic phase was dried with Na_2SO_4 and reduced in vacuum to 3 mL. An oil was precipitated by addition of a mixture of thf (5 mL) and Et_2O (50 mL). For purification, the remaining oil was dissolved in MeCN (5 mL) and again precipitated with thf (10 mL) and Et_2O (25 mL). This procedure had to be repeated approximately three times until the oil solidifies. The so obtained purified violet solid was washed with thf (3 × 10 mL) and dried in vacuum. Yield: 1.37g (0.8 mmol, 76 % based on **7c**).

7c: Anal. Calcd for $C_{88}H_{156}N_{10}O_{14}Cu_2$ (1705.33): C, 61.98; H, 9.22; N, 8.21 %. Found: C, 61.82; H, 9.88; N, 7.88 %. Although these results are outside the range viewed as establishing analytical purity, they are provided to illustrate the best values obtained to date. IR (KBr): $\tilde{\upsilon}$ [cm^{-1}] 3288 (w), 2962 (s), 2934 (m), 2875 (m), 1677 (m), 1625 (vs), 1581 (s), 1555 (m), 1479 (s), 1433 (w), 1382 (w), 1313 (m), 1289 (m), 885 (w), 782 (w), 741 (w). UV/Vis (MeCN): λ_{max} [nm] (ε [l mol^{-1} cm^{-1}]) ca. 212 (sh) (53772), 243 (33352), 279 (39096), ca. 289 (sh) (37200), 339 (31304), 563 (411). MS (ESI-TOF, negative, MeCN): *m/z* = 610.2337 [**9c** – $2Bu_4N$]$^{2-}$ (100 %); 1221.4758 [**9c** – $2Bu_4N$ + H]$^-$ (8 %); 1462.7529 [**9c** – Bu_4N]$^-$ (26 %); 2155.8899 [**9c** – $2Bu_4N$ + Na]$^-$ (14 %). Figure S6† displays the IR spectrum, Figure S55† displays ESI-MS spectrum of **9c**.

Synthesis of $[Bu_4N]_6[den^{III}\{Cu(3,4\text{-}bopb)\}_3]$ (9d). Compound **7d** (1.01 g, 0.74 mmol) was reacted with [Bu_4N]OH (5.81 g, 8.96 mmol, 40% in H_2O) and **2a** (378 mg, 2.22 mmol) under the same reaction conditions described for **9c**. The reaction time after the addition of **2a** was prolonged to 4 h. Compound **9d** could be isolated as violet solid after appropriate work-up, *cf.* remarks given for **9c**. Yield: 1.47 g (0.52 mmol, 70 % based on **7d**).

9d: Anal. Calcd for $C_{144}H_{255}N_{19}O_{24}Cu_3$ (2827.32): C, 61.17; H, 9.09; N, 9.41 %. Found: C, 60.86; H, 9.59; N, 9.03 %. IR (KBr): $\tilde{\upsilon}$ [cm^{-1}] 3283 (w), 2962 (s), 2934 (m), 2875 (m), 1674 (m), 1630 (vs), 1580 (s), 1554 (m), 1480 (s), 1433 (m), 1396 (m), 1382 (m), 1308 (m), 1291 (m), 978 (w), 884 (m), 782 (m), 741 (m). UV/Vis (MeCN): λ_{max} [nm] (ε [l mol^{-1} cm^{-1}]) ca. 211 (sh) (83430), 242 (48740), 279 (55020), ca. 288 (sh) (51130), 338 (45690), 562 (660). MS (ESI-TOF, negative, MeCN): *m/z* = 597.2344 [Cu(3,4-bopb)NH + Bu_4N + H]$^-$ (100%); 838.5114 [Cu(3,4-bopb)NH + $2Bu_4N$ + H]$^-$ (43 %); 1170.5743 [**9d** – $2Bu_4N$]$^{2-}$ (20 %). Figure S6† displays the IR spectrum, Figure S56† displays ESI-MS spectrum of **9d**.

Synthesis of $[Bu_4N]_{10}[den^{V}\{Cu(3,4\text{-}bopb)\}_5]$ (9e). Compound **7e** (441 mg, 0.19 mmol) was reacted with [Bu_4N]OH (2.46 g, 3.78 mmol; 40% in H_2O) and **2a** (160 mg, 0.94 mmol) under

the same reaction conditions described for **9c**. The reaction time after the addition of **2a** was prolonged to 24 h. Compound **9e** could be isolated as violet solid after appropriate work-up, *cf.* remarks given for **9c**. Yield: 729 mg (0.15 mmol, 79 % based on **7e**).

9e: Anal. Calcd for $C_{244}H_{433}N_{33}O_{40}Cu_5 \cdot 6H_2O$ (4895.07): C, 59.87; H, 9.16; N, 9.44 %. Found: C, 59.24; H, 9.24; N, 9.29 %. IR (KBr): $\tilde{\upsilon}$ [cm^{-1}] 3430 (s, br), 3290 (m, br), 2962 (s), 2936 (m), 2932 (m), 2875 (s), 1676 (m), 1630 (vs), 1580 (s), 1554 (s), 1479 (s), 1400 (m), 1376 (m), 1290 (m), 978 (w), 882 (w), 781 (m). UV/Vis (MeCN): λ_{max} [nm] (ε [l mol^{-1} cm^{-1}]) ca. 212 (sh) (166209), 279 (121051), ca. 288 (sh) (109221), 335 (150763), 563 (1212). MS (ESI-TOF, positive, MeOH): *m/z* = 2394.4775 [**9e** + 2H]$^{2+}$ (73 %); 2515.1162 [**9e** + Bu_4N^+ + H]$^{2+}$ (100 %); 2635.7549 [**9e** + $2Bu_4N$]$^{2+}$ (70 %). Figure S6† displays the IR spectrum, Figure S57† displays ESI-MS spectrum of **9e**.

Synthesis of $[Bu_4N]_{20}[den^X\{Cu(3,4\text{-}bopb)\}_{10}]$ (9f). Compound **7f** (274 mg, 0.05 mmol) was reacted with $[Bu_4N]OH$ (1.40 g, 2.16 mmol, 40% in H_2O) and **2a** (94 mg, 0.55 mmol) under the same reaction conditions as described for **9c**. The reaction time after the addition of **2a** was prolonged to 24 h. Compound **9f** could be isolated as violet solid after appropriate work-up, *cf.* remarks given for **9c**. To ensure the purification and for removing of possible side products, the precipitation with thf/Et_2O was stopped at a point, when the solution was still purple. Yield: 263 mg (0.03 mmol, 48 % based on **7f**).

9f: Anal. Calcd for $C_{509}H_{903}N_{73}O_{85}Cu_{10} \cdot 7H_2O$ (10329.76): C, 59.18; H, 9.12; N, 9.90 %. Found: C, 59.29; H, 8.90; N, 9.29 %. Although these results are outside the range viewed as establishing analytical purity, they are provided to illustrate the best values obtained to date. IR (KBr): $\tilde{\upsilon}$ [cm^{-1}] 3446 (m, br), 3280 (m, br), 2962 (s), 2930 (s), 2875 (m), 1675 (s), 1634 (vs), 1580 (s), 1554 (m), 1479 (m), 1396 (m), 1381 (m), 1292 (m), 880 (w), 782 (w). UV/Vis (MeCN): λ_{max} [nm] (ε [l mol^{-1} cm^{-1}]) ca. 212 (sh) (324234), 279 (225678), ca. 288 (sh) (204185), 336 (150763), 562 (2460). Figure S6† displays the IR spectrum of **9f**, Figure S58† the ESI-MS spectra of **9f**.

Synthesis of $[en^{II}\{Cu_3(3,4\text{-}bopb)(pmdta)_2\}_2][BF_4]_4$ (10c). To **9c** (466 mg, 0.27 mmol) dissolved in MeCN (50 mL) a solution of **2d** (449 mg, 0.11 mmol) in MeCN (50 mL) was added drop-wise and stirring was continued for 24 h at ambient temperature. The obtained solution was reduced in vacuum to 5 mL and a green solid precipitated by addition of thf (10 mL). After filtration, the obtained solid was dissolved in MeCN (5 mL), again precipitated by addition of Et_2O (20 mL) and filtered. This procedure had to be repeated three to four times

until the solid became insoluble in MeCN. The thus obtained solid was again redissolved in a mixture of MeCN (3 mL) and DMF (2 mL) and again precipitated with Et_2O (20 mL). The purified green solid was then carefully washed with Et_2O (3 × 20 mL) and dried in vacuum. Yield: 198 mg (0.1 mmol, 35 % based on **9c**).

10c: Anal. Calcd for $C_{60}H_{104}B_4N_{18}O_{14}F_{16}Cu_6$ (2030.07): C, 35.50; H, 5.16; N, 12.42 %. Found: C, 36.35; H, 5.24; N, 12.30 %. Although these results are outside the range viewed as establishing analytical purity, they are provided to illustrate the best values obtained to date. IR (KBr): $\tilde{\upsilon}$ [cm^{-1}] 3006 (w), 2973 (w), 2930 (w), 2883 (w), 2846 (w), 2802 (w), 1627 (vs), 1583 (s), 1475 (m), 1342 (m), 1260 (w), 1084 (m), 1053 (m), 870 (w), 809 (w), 778 (w). MS (ESI-TOF, positive, MeCN): *m/z* = 420.5928 [**10c** – $4BF_4$]$^{4+}$ (15 %); 635.5326 [**10c** – Cu(pmdta) – pmdta – $4BF_4$]$^{2+}$ (100 %). UV/Vis (DMSO): λ_{max} [nm] (ε [l mol^{-1} cm^{-1}]) 276 (58650), ca. 340 (sh) (7188), 658 (1308). Figure S7† displays the IR spectrum, Figure S59† the ESI-MS spectrum of **10c**.

Synthesis of [den^{III}{Cu_3(3,4-bopb)(pmdta)$_2$}$_3$][BF_4]$_6$ (10d). Compound **9d** (209 mg, 0.07 mmol) was reacted with **2d** (182 mg, 0.44 mmol) under the same reaction conditions as described for the synthesis of **10c**. After stirring for 2 d and appropriate work-up, *cf.* remarks given for **10c**, **10d** could be isolated as green solid. Yield: 100 mg (0.03 mmol, 41% based on **9d**).

10d: Anal. Calcd for $C_{102}H_{177}N_{31}O_{24}B_6F_{24}Cu_9$ (3314.43): C, 36.96; H, 5.38; N, 13.10 %. Found: C, 36.68; H, 5.41; N, 13.44 %. IR (KBr): $\tilde{\upsilon}$ [cm^{-1}] 3422 (s), 2973 (w), 2932 (w), 2881 (w), 1627 (vs), 1474 (m), 1340 (w), 1260 (w), 1084 (s), 1054 (s). UV/Vis (DMSO): λ_{max} [nm] (ε [l mol^{-1} cm^{-1}]) 284 (122277), 292 (122319), ca. 322 (sh) (86999), 658 (1935d). MS (ESI-TOF, positive, MeCN): *m/z* = 476.8834 [**10d** – Cu(pmdta) – pmdta – $6BF_4$ + H]$^{5+}$ (10 %); 595.8524 [**10d** – Cu(pmdta) – pmdta – $6BF_4$]$^{4+}$ (60 %); 715.4341 [**10d** – 2Cu(pmdta) – pmdta – $6BF_4$ + H]$^{3+}$ (100 %); 1072.6476 [**10d** – 2Cu(pmdta) – pmdta – $6BF_4$]$^{2+}$ (13 %). Figure S7† displays the IR spectrum, Figure S60† displays ESI-MS spectrum of **10d**.

Synthesis of [den^{V}{Cu_3(3,4-bopb)(pmdta)$_2$}$_5$][BF_4]$_{10}$ (10e). Compound **9e** (193 mg, 0.04 mmol) was reacted with **2d** (165 mg, 0.4 mmol) under the same reaction conditions as described for the synthesis of **10c**. After stirring for 2 d and appropriate work-up, *cf.* remarks given for **10c**, **10e** could be isolated as green solid. Yield: 113 mg (0.02 mmol, 50% based on **9e**).

10e: Anal. Calcd for $C_{175}H_{307}B_{10}N_{53}O_{40}F_{40}Cu_{15}$ (5598.84): C, 37.33; H, 5.45; N, 13.26 %. Found: C, 36.87; H, 5.54; N, 11.98 %. IR (KBr): $\tilde{\upsilon}$ [cm^{-1}] 3413 (s), 2973 (w), 2932 (w), 2884 (w), 1627 (vs), 1474 (m), 1345 (w), 1054 (s). UV/Vis (DMSO): λ_{max} [nm] (ε [l mol^{-1} cm^{-1}]) 286 (170722), 293 (170793), ca. 318 (sh) (123215), 661 (3155). MS (ESI-TOF, positive, H_2O/MeCN): *m/z* = 874.8365 [**10e** – 3Cu(pmdta) – 3(pmdta) – $10BF_4$]$^{4+}$ (100 %); 1021.2128 [**10e** – 2Cu(pmdta) – pmdta – $10BF_4$ + H]$^{4+}$ (41 %); 1195.4500 [**10e** – 3Cu(pmdta) – 3pmdta – $9BF_4$]$^{3+}$ (70 %). Figure S7† displays the IR spectrum, Figure S61† displays ESI-MS spectrum of **10e**.

Synthesis of [den^{X}{Cu_3(3,4-bopb)(pmdta)$_2$}$_3$][BF_4]$_{20}$ (10f). Compound **9f** (107 mg, 0.01 mmol) was reacted with **2d** (90 mg, 0.22 mmol) under the same reaction conditions as described for the synthesis of **10c**. After stirring for 2 d and appropriate work-up, *cf.* remarks given for **10c**, **10f** could be isolated as green solid. Yield: 70 mg (0.01 mmol, 56 % based on **9f**).

10f: Anal. Calcd for $C_{369}H_{643}N_{113}O_{85}B_{20}F_{80}Cu_{30}$ (11665.24): C, 37.99; H, 5.56; N, 13.57 %. Found: C, 37.11; H, 5.92; N, 12.54 %. Although these results are outside the range viewed as establishing analytical purity, they are provided to illustrate the best values obtained to date. IR (KBr): $\tilde{\upsilon}$ [cm^{-1}] 3414 (s), 2974 (m), 2934 (m), 2901 (m), 2878 (m), 1627 (vs), 1474 (m), 1345 (w), 1249 (w), 1054 (s). UV/Vis (DMSO): λ_{max} [nm] (ε [l mol^{-1} cm^{-1}]) 286 (384940), 293 (385964), ca. 317 (sh) (277722), 658 (6703). MS (ESI-TOF, positive, MeCN): *m/z* = 414.5875 [{Cu_3(3,4-bopbNH)(pmdta)$_2$} + 2H]$^{2+}$ (99 %); 735.0983 (100 %); 1089.0816 [1**0f** – 9Cu(pmdta) – pmdta + 15H]$^{7+}$ (7 %). Figure S7† displays the IR spectrum, Figure S62† the ESI-MS spectrum of **10f**.

Acknowledgement

This work has been supported by the Deutsche Forschungsgemeinschaft through project FOR 1154 “Towards Molecular Spintronics”.

References

1 D. A. Tomalia, H. Baker, J. Dewald, M. Hall, G. Kallos, S. Martin, J. Roeck, J. Ryder and P. Smith, *Polym. J.*, 1985, 17, 117–132.

2 F. Zeng and S. C. Zimmerman, *Chem. Rev.*, 1997, **97**, 1681–1712.

3 C. J. Hawker and J. M. J. Frechet, *J. Am. Chem. Soc.*, 1990, **112**, 7638–7647.

4 D. Astruc, E. Boisselier and C. Ornelas, *Chem. Rev.*, 2010, **110**, 1857–1959.

5 F. Vögtle, G. Richardt and N. Werner, *Dendritische Moleküle Konzepte, Synthesen, Eigenschaften, Anwendungen*, B.G. Teubner Verlag, Wiesbaden, 1st edn., 2007.

6 D. A. Tomalia, *New. J. Chem.*, 2012, **36**, 264–281.

7 H.-F. Chow, C.-F. Leung, G.-X. Wang and Y.-Y. Yang, *Comptes Rendus Chim.*, 2003, **6**, 735–745.

8 J.-J. Lee, W. T. Ford, J. A. Moore and Y. Li, *Macromolecules*, 1994, **27**, 4632–4634.

9 C. Francavilla, F. V. Bright and M. R. Detty, *Org. Lett.*, 1999, **1**, 1043–1046.

10 R. Breinbauer and E. N. Jacobsen, *Angew. Chem. Int. Ed.*, 2000, **39**, 3604–3607.

11 A. W. Kleij, R. a Gossage, J. T. B. H. Jastrzebski, J. Boersma and G. Van Koten, *Angew. Chem. Int. Ed.*, 2000, **3**, 176–178.

12 G. Pistolis, A. Malliaris, D. Tsiourvas and C. M. Paleos, *Chem. - A Eur. J.*, 1999, **5**, 1440–1444.

13 L. J. Twyman, A. E. Beezer, R. Esfand, M. J. Hardy and J. C. Mitchell, *Tetrahedron Lett.*, 1999, **40**, 1743–1746.

14 G. R. Newkome, R. Güther, C. N. Moorefield, F. Cardulla, L. Echegoyen, E. Perez-Cordero and H. Luftmann, *Angew. Chem. Int. Ed.*, 1995, **34**, 2023–2026.

15 H.-F. Chow, I. Y. K. Chan, D. T. W. Chan and R. W. M. Kwok, *Chem. - A Eur. J.*, 1996, **2**, 1085–1091.

16 D. L. Stone, D. K. Smith and P. T. McGrail, *J. Am. Chem. Soc*, 2002, **124**, 856–864.

17 C. M. Cardona and A. E. Kaifer, *J. Am. Chem. Soc.*, 1998, **120**, 4023–4024.

18 S. Mattei, P. Wallimann, B. Kenda, W. Amrein and F. Diederich, *Helv. Chim. Acta*, 1997, **80**, 2391–2417.

19 C. A. Schalley, C. Verhaelen, F.-G. Klärner, U. Hahn and F. Vögtle, *Angew. Chemie*, 2005, **117**, 481–485.

20 S. a. Vinogradov, L. W. Lo and D. F. Wilson, *Chem. - A Eur. J.*, 1999, **5**, 1338–1347.

21 B. Helms and J. M. J. Fréchet, *Adv. Synth. Catal.*, 2006, **348**, 1125–1148.

22 A.-M. Caminade, A. Ouali, R. Laurent, C.-O. Turrin and J.-P. Majoral, *Chem. Soc. Rev.*, 2015, **44**, 3890–3899.

23 P. Neumann, H. Dib, A.-M. Caminade and E. Hey-Hawkins, *Angew. Chem. Int. Ed.*, 2015, **54**, 311–314.

24 M. R. Knecht and R. M. Crooks, *New J. Chem.*, 2007, **31**, 1349–1353.

25 M. R. Knecht, J. C. Garcia-Martinez and R. M. Crooks, *Chem. Mater.*, 2006, **18**, 5039–5044.

26 S. Dietrich, S. Chandra, C. Georgi, S. Thomas, D. Makarov, S. Schulze, M. Hietschold, M. Albrecht, D. Bahadur and H. Lang, *Mater. Chem. Phys.*, 2012, **132**, 292–299.

27 M. L. Tran, L. R. Gahan and I. R. Gentle, *J. Phys. Chem. B*, 2004, **108**, 20130–20136.

28 D. Appelhans, U. Oertel, R. Mazzeo, H. Komber, J. Hoffmann, S. Weidner, B. Brutschy, B. Voit and M. FrancescaOttaviani, *Proc. R. Soc. A Math. Phys. Eng. Sci.*, 2010, **466**, 1489–1513.

29 X. G. Lei, S. Jockusch, N. J. Turro, D. a. Tomalia and M. F. Ottaviani, *J. Colloid Interface Sci.*, 2008, **322**, 457–464.

30 S. D. Swanson, J. F. Kukowska-Latallo, A. K. Patri, C. Chen, S. Ge, Z. Cao, A. Kotlyar, A. T. East and J. R. Baker, *Int. J. Nanomedicine*, 2008, **3**, 201–210.

31 Z. Cheng, D. L. J. Thorek and A. Tsourkas, *Angew. Chem. Int. Ed.*, 2010, **49**, 346–350.

32 D. Astruc, F. Lu and J. R. Aranzaes, *Angew. Chemie*, 2005, **117**, 8062–8083.

33 M. Zhao and R. Crooks, *Angew. Chem. Int. Ed.*, 1999, **38**, 364–366.

34 S. Sun, *Adv. Mater.*, 2006, **18**, 393–403.

35 A. Ethirajan, U. Wiedwald, H. G. Boyen, B. Kern, L. Han, A. Klimmer, F. Weigl, G. Kästle, P. Ziemann, K. Fauth, J. Cai, R. J. Behm, A. Romanyuk, P. Oelhafen, P. Walther, J. Biskupek and U. Kaiser, *Adv. Mater.*, 2007, **19**, 406–410.

36 B. Lohse, R. Vestberg, M. T. Ivanov, S. Hvilsted, R. H. Berg, P. S. Ramanujam and C. J. Hawker, *J. Polym. Sci. Part A Polym. Chem.*, 2007, **45**, 4401–4412.

37 H. Bin Na, I. C. Song and T. Hyeon, *Adv. Mater.*, 2009, **21**, 2133–2148.

38 L. Babes, B. Denizot, G. Tanguy, Le Jeune JJ and P. Jallet, *J. Colloid Interface Sci.*, 1999, **212**, 474–482.

39 H. Kobayashi and M. W. Brechbiel, *Adv. Drug Deliv. Rev.*, 2005, **57**, 2271–2286.

40 H. Kobayashi, S. Kawamoto, S. K. Jo, H. L. Bryant, M. W. Brechbiel and R. a. Star, *Bioconjug. Chem.*, 2003, **14**, 388–394.

41 A. K. Diallo, C. Ornelas, L. Salmon, J. R. Aranzaes and D. Astruc, *Angew. Chem. Int. Ed.*, 2007, **46**, 8644–8648.

42 Y. Niu and R. M. Crooks, *Comptes Rendus Chim.*, 2003, **6**, 1049–1059.

43 C. Paul-Roth, *Comptes Rendus Chim.*, 2005, **8**, 1232–1236.

44 O. Kahn, *Adv. Inorg. Chem.*, 1995, **43**, 179–260.

45 O. Kahn, *Molecular Magnetism*, VCH, Weinheim, 1st edn., 1993.

46 J. S. Miller and A. J. Epstein, *MRS Bull.*, 2000, 21–28.

47 E. Pardo, R. Ruiz-García, J. Cano, X. Ottenwaelder, R. Lescouëzec, Y. Journaux, F. Lloret and M. Julve, *Dalton Trans.*, 2008, 2780–805.

48 H. Stumpf, L. Ouahab, Y. Pei, D. Grandjean and O. Kahnt, *Science*, 1993, **261**, 447–449.

49 E. Pardo, R. Ruiz-García, F. Lloret, M. Julve, J. Cano, J. Pasán, C. Ruiz-Pérez, Y. Filali, L.-M. Chamoreau and Y. Journaux, *Inorg. Chem.*, 2007, **46**, 4504–4514.

50 A. Aukauloo, X. Ottenwaelder, R. Ruiz, Y. Journaux, Y. Pei, E. Rivière and M. C. Muñoz, *Eur. J. Inorg. Chem.*, 2000, **2000**, 951–957.

51 X. Ottenwaelder, J. Cano, Y. Journaux, E. Rivière, C. Brennan, M. Nierlich and R. Ruiz-García, *Angew. Chem. Int. Ed.*, 2004, **43**, 850–852.

52 A. Aukauloo, X. Ottenwaelder, R. Ruiz, Y. Journaux, Y. Pei, E. Riviere, B. Cervera and M. C. Munoz, *Eur. J. Inorg. Chem*, 1999, 209–212.

53 M. Kalisz, M. a Novak, C. B. Pinheiro, A. S. Florencio, G. Chapuis, A. Caneschi and M. G. F. Vaz, 2007, **18**, 916–923.

54 A. Aukauloo, X. Ottenwaelder, R. Ruiz, S. Poussereau, Y. Pei, Y. Journaux, P. Fleurat, F. Volatron, B. Cervera and M. C. Munoz, *Eur. J. Inorg. Chem*, 1999, 1067–1071.

55 T. Mallah, S. Parsons and D. Messenger, *Priv. Commun.*, 2005.

56 E. Pardo, J. Faus, M. Julve, F. Lloret, M. C. Munoz, J. Cano, X. Ottenwaelder, Y. Journaux, R. Carrasco, G. Blay, I. Fermandez and R.-G. R., *J.Amer.Chem.Soc.*, 2003, **125**, 10770–10771.

57 J. Ferrando-Soria, M. Castellano, R. Ruiz-García, J. Cano, M. Julve, F. Lloret, C. Ruiz-Pérez, J. Pasán, L. Cañadillas-Delgado, D. Armentano, Y. Journaux and E. Pardo, *Chem. - A Eur. J.*, 2013, **19**, 12124–12137.

58 J. Ferrando-Soria, M. Castellano, R. Ruiz-García, J. Cano, M. Julve, F. Lloret, J. Pasán, C. Ruiz-Pérez, L. Cañadillas-Delgado, Y. Li, Y. Journaux and E. Pardo, *Chem. Commun.*, 2012, **48**, 8401–8403.

59 E. Pardo, R. Carrasco, R. Ruiz-Garcia, M. Julve, F. Lloret, M. C. Muñoz, Y. Journaux, E. Ruiz and J. Cano, *J. Am. Chem. Soc.*, 2008, **130**, 576–585.

60 M. Castellano, J. Ferrando-Soria, E. Pardo, M. Julve, F. Lloret, C. Mathonière, J. Pasán, C. Ruiz-Pérez, L. Cañadillas-Delgado, R. Ruiz-García and J. Cano, *Chem. Commun.*, 2011, **47**, 11035–11037.

61 M. Castellano, R. Ruiz-García, J. Cano, M. Julve, F. Lloret, Y. Journaux, G. De Munno and D. Armentano, *Chem. Commun.*, 2013, **49**, 3534–3536.

62 M. Castellano, F. R. Fortea-Pérez, S. E. Stiriba, M. Julve, F. Lloret, D. Armentano, G. De Munno, R. Ruiz-Garci and J. Cano, *Inorg. Chem.*, 2011, **50**, 11279–11281.

63 W. D. do Pim, W. X. C. Oliveira, M. a Ribeiro, É. N. de Faria, I. F. Teixeira, H. O. Stumpf, R. M. Lago, C. L. M. Pereira, C. B. Pinheiro, J. C. D. Figueiredo, W. C. Nunes, P. P. de Souza, E. F. Pedroso, M. Castellano, J. Cano and M. Julve, *Chem. Commun.*, 2013, **49**, 10778–10780.

64 M. C. Dul, X. Ottenwaelder, E. Pardo, R. Lescouezëc, Y. Journaux, L. M. Chamoreau, R. Ruiz-García, J. Cano, M. Julve and F. Lloret, *Inorg. Chem.*, 2009, **48**, 5244–5249.

65 E. Pardo, K. Bernot, M. Julve, F. Lloret, J. Cano, R. Ruiz-Garcia, F. S. Delgado, C. Ruiz-Perez, X. Ottenwaelder and Y. Journaux, *Inorg. Chem.*, 2004, **43**, 2768–2770.

66 M. C. Dul, J. Ferrando-Soria, E. Pardo, R. Lescouëzec, Y. Journaux, R. Ruiz-García, J. Cano, M. Julve, F. Lloret, O. Fabelo, J. Pasán and C. Ruiz-Pérez, *Inorg. Chem.*, 2010, **49**, 11264–11266.

67 I. Fernandez, R. Ruiz, J. Faus, M. Julve, F. Lloret, J. Cano, X. Ottenwaelder, Y. Journaux and M. C. Munoz, *Angew. Chem. Int. Ed.*, 2001, **1**, 3039–3042.

68 E. Pardo, J. Ferrando-Soria, M. C. Dul, R. Lescouëzec, Y. Journaux, R. Ruiz-García, J. Cano, M. Julve, F. Lloret, L. Cañadillas-Delgado, J. Pasán and C. Ruiz-Pérez, *Chem. - A Eur. J.*, 2010, **16**, 12838–12851.

69 R. Ruiz, C. Surville-Barland, A. Aukauloo, E. Anxolabehere-Mallart, Y. Journaux and M. C. Muñoz, *J. Chem. Soc., Dalton Trans*, 1997, 745–751.

70 T. Rüffer, B. Bräuer, A. K. Powell, I. Hewitt and G. Salvan, *Inorg. Chim. Acta*, 2007, **360**, 3475–3483.

71 R. O. Al-Kaysi, R. J. Dillon, J. M. Kaiser, L. J. Mueller, G. Guirado and C. J. Bardeen, *Macromolecules*, 2007, **40**, 9040–9044.

72 J. Artacho, E. Ascic, T. Rantanen, J. Karlsson, C. J. Wallentin, R. Wang, O. F. Wendt, M. Harmata, V. Snieckus and K. Wärnmark, *Chem. - A Eur. J.*, 2012, **18**, 1038–1042.

73 N. V Likhanova, I. V Lijanova, L. P. M. Alvarado, M. M. García, S. Hernández-Ortega and O. O. Xometl, *Curr. Org. Chemsitry*, 2013, **17**, 79–82.

74 K. Holmberg and B. Hansen, *Tetrahedron*, 1975, **27**, 2303–2306.

75 F. Eya'ane Meva, D. Schaarschmidt, M. a. Abdulmalic and T. Rüffer, *Acta Crystallogr. Sect. E Struct. Reports Online*, 2012, **68**, o3460–o3461.

76 T. Rüffer, B. Bräuer, F. E. Meva and B. Walfort, *Dalton Trans.*, 2008, 5089–5098.

77 G. A. Olah, M. Nojima and I. Kerekes, *Synthesis*, 1973.

78 L. A. Carpino, D. Sadat-Aalaee, H. G. Chao and R. H. DeSelms, *J. Am. Chem. Soc*, 1990, **112**, 9651–9652.

79 C. Chen, C. Chien and C. Su, *J. Fluor. Chem.*, 2002, **115**, 75–77.

80 C. A. G. N. Montalbetti and V. Falque, *Tetrahedron*, 2005, **61**, 10827–10852.

81 D. A. Tomalia, *United States Patent 4507466, 1985.*, United States, 1985.

82 S. Dietrich, A. Nicolai and H. Lang, *J. Organomet. Chem.*, 2011, **696**, 739–747.

83 M. W. P. L. Baars and E. W. Meijer, *Dendrimers II, Architecture, Nanostructure and Supramolecular Chemistry*, Springer Verlag, Berlin, 2000.

84 T. Li, K. Hong, L. Porcar, R. Verduzco, D. Butler, G. S. Smith, Y. Liu, W.-R. Chen and P. D. Butler, *Macromolecules*, 2008, **41**, 8916–8920.

85 C. N. R. Rao, *Ultra-Violet and VISible Spectroscopy Chemical Applications*, Butterworths, London, 3rd Editio., 1975.

86 E. Clar, *Aromatische Kohlenwaserstoffe*, Springer Verlag, Berlin, 1952.

87 M. Hesse, H. Meier and B. Zeeh, *Spektroskopische Methoden in der organischen Chemie*, Georg Thieme Verlag, Stuttgart, 5th edn., 1995.

88 B. Cervera, J. L. Sanz, M. J. Ibáñez, G. Vila, F. LLoret, M. Julve, R. Ruiz, X. Ottenwaelder, A. Aukauloo, S. Poussereau, Y. Journaux and M. C. Muñoz, *J. Chem. Soc. Dalton Trans.*, 1998, 781–790.

89 X. Ottenwaelder, A. Aukauloo, Y. Journaux, R. Carrasco, J. Cano, B. Cervera, I. Castro, S. Curreli, M. C. Muñoz, A. L. Roselló, B. Soto and R. Ruiz-García, *Dalton Trans.*, 2005, 2516–26.

90 A. B. P. Lever, *Inorganic Electronic Spectroscopy*, Elsevier Publishing Company, Amsterdam, London, New York, 1st edn., 1968.

91 E.-Q. Gao, Q.-H. Zhao, J.-K. Tang, D.-Z. Liao, Z.-H. Jiang and S.-P. Yan, *J. Chem. Soc. Dalton Trans.*, 2001, **3**, 1537–1540.

92 Q.-L. Wang, D.-Z. Liao, S.-P. Yan, Z.-H. Jiang, P. Cheng and Q. Zr, *Chinese J. Chem.*, 2002, **20**, 1249–1255.

93 G. Zheng, Baomeng, Q. Wang, G. Zhang and Shiqiang, *Synth. React. Inorg. Met. Chem.*, 1999, **29**, 855–864.

94 M. A. Abdulmalic, A. Aliabadi, A. Petr, Y. Krupskaya, V. Kataev, B. Büchner, R. Zaripov, E. Vavilova, V. Voronkova, K. Salikov, T. Hahn, J. Kortus, F. Eya'ane Meva, D. Schaarschmidt and T. Rüffer, *Dalton Trans.*, 2015, **44**, 8062–8079.

95 T. Rüffer, B. Bräuer and B. Walfort, *Inorg. Chem. Commun.*, 2006, **9**, 1111–1113.

96 Z. C. Zhu, X. P. Mao, Z. Xu and X. Y. Huang, *Chin. J. Struct. Chem.*, 2000, **19**, 322–325.

97 M. A. Abdulmalic, A. Aliabadi, A. Petr, V. Kataev and T. Rüffer, *Dalton Trans.*, 2013, **42**, 1798–1809.

98 R. D. Shannon, *Acta Crystallogr., Sect. A Cryst. Phys., Diffr., Theor. Gen. Cryst.*, 1976, **32**, 751–767.

99 L. Banci, A. Bencini and D. Gatteschi, *Inorg. Chem.*, 1983, **22**, 2681–2683.

100 M. A. Abdulmalic, A. Aliabadi, A. K. Petr, Y. Krupskaya, V. Kataev, B. Büchner, T. Hahn, J. Kortus, N. Yèche, H.-H. H. H. Klauss, T. Rüffer, B. Bu, T. Hahn, J. Kortus, N. Yeche, H.-H. H. H. Klauss and T. Rüffer, *Organometallics*, 2013, **32**, 5988–6003.

101 M. A. Abdulmalic, A. Aliabadi, A. Petr, Y. Krupskaya, V. Kataev, B. Büchner, T. Hahn, J. Kortus and T. Rüffer, *Dalton Trans.*, 2012, **41**, 14657–14670.

102 http://www.mpibac.mpg.de/bac/index_en.php/logins/bill/julX_en.php.

103 R. Costa, A. Garcia, J. Ribas, T. Mallah, Y. Journaux, J. Sletten, X. Solans and V. Rodrfguez, *Inorg. Chem.*, 1993, **32**, 3733–3742.

104 R. Costa, A. Garcia, R. Sanchez, J. Ribas, X. Solans and V. Rodriguez, *Polyhedron*, 1993, **12**, 2697–2704.

105 D. D. Perrin and W. L. F. Armarego, *Purification of Laboratory Chemicals Pergamon*, New York, 3rd Editio., 1988.

106 J. Kühnert, T. Rüffer, P. Ecorchard, B. Bräuer, Y. Lan, A. K. Powell and H. Lang, *Dalton Trans.*, 2009, 4499–4508.

107 R. T. Weber, J. J. Jiang and D. Barr, *EPR Division*, Bruker Instruments, Inc., Software Version 2.3, Software V., 1998.

108 W. Simfonia, *a fast, easy to use EPR spectral simulation*, Bruker Analytical Instruments GmBH, Software Version 1.25, 1996.

109 G. M. Sheldrick, *Acta Cryst*, 2008, **A64**.